Glacial dust surpasses both volcanic ash and desert dust in its iron fertilization potential

Bess G. Koffman[1], Meg F. Yoder[1,2], Taylor Methven[1], Lena Hanschka[1], Helen B. Sears[1], Patrick L. Saylor[3,4], Kristi L. Wallace[5]

[1]Department of Geology, Colby College, Waterville, ME 04901
[2]Department of Earth and Environmental Sciences, Boston College, Boston, MA 02467
[3]Cold Regions Research and Engineering Laboratory, Hanover, NH 03755
[4]Earth Science Department, Dartmouth College, Hanover, NH 03755
[5]USGS Volcano Science Center, Anchorage, AK 99508

For submission to *Global Biogeochemical Cycles*, summer 2020

Keywords: Dust, volcanic ash, trace metals, iron fertilization, iron solubility, Alaska

Key Points:

1) Alaska glacial sediments contain easily-reducible Fe that is 5x higher than Asian desert sediments and 14x higher than volcanic ash.
2) Iron in volcanic ash is relatively insoluble and non-bioavailable.
3) Sediment and volcanic ash Fe availability increases through time and environmental exposure in the climate of southcentral Alaska.
4) Alaska glacier-derived sediments contain five to thirty times higher Cu, Ni, and Pb, and ~twice as high Co, Zn, Cd, and Mo as volcanic ash.

Abstract

The subarctic Pacific Ocean and Bering Sea comprise the second-largest high nitrate, low chlorophyll region in the world, where primary production is limited by the availability of iron (Fe). To estimate the potential impact of different terrestrial aerosol Fe sources on marine ecosystems, we performed a suite of laboratory assessments following established protocols, including: 1) leaching with Milli-Q water, 2) sequential extractions, 3) complete acid digestions, 4) X-ray diffraction, and 5) grain size analysis. Measurements were performed on 20 fine-grained (<5 μm) glacier-derived sediments from Alaska and the Yukon, 2 fresh, never-wetted volcanic ashes (Redoubt 2009 and Pavlof 2016), and 6 weathered ashes (Redoubt and Augustine) which span the past ~8700 years. We compared results to published data on Asian desert-derived sediments, finding that the glacier-derived sediments have five times higher easily-reducible Fe (median 2.3 ± 0.6 wt. %) than desert-derived samples (0.49 ± 0.1 wt. %) and fourteen times higher easily-reducible Fe than fresh ash (0.16 ± 0.1 wt. %). In addition, fractional Fe solubility was higher in glacial sediment (median cumulative 0.31 ± 0.11% Fe_S) than volcanic ash (0.04 ± 0.02 % Fe_S). Glacial sediments also contained higher concentrations of bioactive metals including Co, Ni, Cu, Zn, Mo, Cd, and Pb. Inferred Fe availability increased with sample age, pointing to the ability of environmental weathering processes to change Fe geochemistry. Together these results suggest that glacier-derived dust may provide the subarctic Pacific with more bioavailable iron per unit mass than either volcanic ash or desert-derived dust.

Plain Language Summary

The subarctic Pacific Ocean is a region where the growth of algae at the base of the ocean's food web is limited by a lack of the nutrient iron. In offshore regions far from river discharge and the edges of continents, iron inputs from the atmosphere, such as from volcanic ash or dust storms, can help fuel algae growth, supporting the ocean ecosystem and fisheries that depend on it. In order to learn how different terrestrial nutrient sources might impact algae growth, we compared the compositions of volcanic ash, dust from Asian deserts, and dust from glacier-fed riverbeds in Alaska and Yukon Territory. We also looked at ash and dust of different ages, to see how compositions changed through time. We found that glacier-derived dust had the most iron in a form usable by algae, nearly five times higher than desert dust and fourteen times higher than volcanic ash. The ash had the lowest amount of iron in a form usable by algae. We also found that the form of iron in both volcanic ash and glacial dust changes with increasing time and environmental exposure in southcentral Alaska's climate, making it more biologically available to algae as it ages.

1. Introduction

The Arctic and subarctic Pacific Ocean is experiencing rapid change as a result of climate warming and associated feedbacks (Gregg et al. 2003; Grebmeier et al. 2006; Serreze et al. 2007). The northeastern Pacific Ocean and the Bering Sea are characterized as high nutrient, low chlorophyll (HNLC) regions due to limited iron (Fe) inputs. Global satellite-based measurements of primary production suggest a large decrease in the North Pacific region (-9.3%) associated with increasing sea surface temperatures and decreasing terrestrial dust deposition, thus enhancing this region's HNLC status (Gregg et al. 2003). Climate change may impact nutrient cycling by affecting sources and availability of Fe and macronutrients to pelagic phytoplankton (e.g., Aguilar-Islas et al. 2008; Kipp et al. 2018). There may also be changes in the seasonality of nutrient deposition, altering the relevance and impact of different terrestrial nutrient sources.

Despite significant progress toward understanding phytoplankton growth response to Fe fertilization, the relative importance of different natural micronutrient sources has not fully been explored. Aerosol geochemistry may play an important role in determining bioavailability and thus stimulating phytoplankton growth and production (Journet et al. 2008; Schroth et al. 2009). Fractional Fe solubility (%Fe_S), operationally defined as the fraction of total Fe that passes

94 through a given filter pore size, has been used as a measure of Fe availability (e.g., Fan et al.
95 2006; Winton et al. 2016). Mineral dust typically has $\%Fe_S$ of 1% (Jickells and Spokes 2001;
96 Mahowald et al. 2009) though higher measured $\%Fe_S$ (~10-90%) worldwide points to a
97 significant soluble Fe contribution from combustion emissions (Chuang et al. 2005; Sedwick et
98 al. 2007; Sholkovitz et al. 2012). Atmospheric processing by acidic aerosols, including industrial
99 pollution, tends to reduce Fe oxidation state, increasing solubility substantially (Cwiertny et al.
100 2008; Solmon et al. 2009). Recent work has suggested that factors besides $\%Fe_S$, such as Fe
101 speciation (Schroth et al. 2009) and oxidation state of particulate Fe, driven by sediment
102 weathering mechanism (Shoenfelt et al. 2017, 2019), may better reflect the Fe available for use
103 by phytoplankton. Thus there is a strong link between the geology and weathering history of
104 mineral aerosols and their potential impact on ocean ecosystems.
105 In addition to Fe, other trace elements needed for phytoplankton growth include
106 manganese (Mn), cobalt (Co), cadmium (Cd), nickel (Ni), copper (Cu), molybdenum (Mo), and
107 zinc (Zn) (Morel 1991; Baeyens et al. 2011; Twining and Baines 2013), which can be co-limiting
108 with iron in HNLC regions. Trace element quotas vary among phytoplankton taxa, but a
109 generalized stoichiometry of their requirements is $Fe \approx Zn > Mn \approx Ni \approx Cu >> Co \approx Cd$
110 (Twining et al. 2011; Twining and Baines, 2013). In addition, trace elements such as Cu, Cd, and
111 lead (Pb) can be toxic to phytoplankton in high concentrations, and terrestrial aerosols are a
112 recognized source of these metals (Paytan et al. 2009; Echeveste et al. 2012).
113 The northeastern subarctic Pacific receives terrestrial nutrients from several sources. It is
114 generally assumed that dust sourced from Asian deserts accounts for the majority of the annual
115 atmospheric Fe deposition, given high annual dust emissions and peak deposition during
116 springtime (Harrison et al. 1999; Xuan and Sokolik 2002; Measures et al. 2005; Mahowald et al.
117 2005, 2009; Fischer et al. 2009). For instance, deposition from the April 2001 "perfect dust
118 storm" caused a near-doubling of carbon biomass over a two-week interval in the northeastern
119 Pacific (Bishop et al. 2002). In contrast to this ongoing, annual supply of dust, volcanic eruptions
120 have been recognized as a significant episodic source of micronutrients in Fe-limited regions
121 (Browning et al. 2014, 2015; Simonella et al. 2015). Notably, direct deposition of ash from the
122 2008 eruption of Kasatochi (Alaska) fueled an anomalous phytoplankton bloom in the Gulf of
123 Alaska (GOA) (Hamme et al. 2010; Langmann et al. 2010), potentially even enhancing salmon
124 recruitment in subsequent years (Parsons and Whitney 2012; Olgun et al. 2013). Ash plumes

125 containing iron-bearing silicate minerals and glass can be dissolved by the low pH of the plume;
126 the dissolved components can then be reprecipitated as highly soluble iron salts, but the degree to
127 which these salts alter the amount of soluble iron in volcanic ash is unknown (Browning et al.
128 2015). Although direct volcanic ash fertilization has thus far only been assessed on a case-by-
129 case basis, such examples hint at a potential ongoing role for intermittent eruptions in natural Fe
130 fertilization of this volcanically active region.

131 Volcanic ash previously deposited sub-aerially can also be remobilized and deposited
132 subsequently in the ocean. Recent satellite observations of ash remobilization from the flanks of
133 Kamchatka (Russia) volcanoes suggest that volcanically-sourced nutrients may be deposited in
134 the surface ocean for months to years following an eruption (Flower and Kahn 2017a). In fact,
135 ash remobilization can continue for decades following large eruptions, a phenomenon most
136 evident at Katmai (Alaska) where remobilization is ongoing (Global Volcanism Program 2016;
137 Wallace and Schwaiger 2018) despite the dormancy of the volcano since 1912 (Hildreth 1983).
138 Aged ash, even though it has likely lost the soluble salts thought to make fresh ash particularly
139 reactive (Jones and Gislason 2008; Duggen et al. 2010), typically exhibits high micronutrient
140 availability relative to desert dust (Frogner et al. 2001; Chuang et al. 2005; Schroth et al. 2009;
141 Duggen et al. 2010). Given that active volcanoes characterize the northern Pacific rim,
142 remobilized volcanic ash may serve as a significant and previously unrecognized ongoing source
143 of nutrients to this Fe-limited ecosystem.

144 A fourth source of terrestrial nutrients, glacially-fed Alaska riverbeds provide a
145 potentially significant supply of mechanically-weathered mineral material to the northeastern
146 subarctic Pacific. Glacially-derived dust plumes have been observed extending from multiple
147 river mouths hundreds of km into the GOA, where they are deposited into the Fe-limited
148 offshore region (Crusius et al. 2011; Schroth et al. 2017). Although these local dust sources do
149 not have the global footprint of Asian desert dust (e.g., Uno et al. 2009), the processes producing
150 the glacial dust, namely, mechanical weathering of bedrock via glacier activity, may make the Fe
151 and other micronutrients more bioavailable than in desert dust (Schroth et al. 2009; Bullard et al.
152 2016; Shoenfelt et al. 2017, 2019). For example, Muhs et al. (2013) found that loess (wind-
153 blown silt) within the Copper River basin of southcentral Alaska, the largest drainage into the
154 GOA, contained a higher proportion of Fe than all other loess bodies in North America.
155 Estimated loess mass accumulation rates (MARs) during the Holocene range from 78–158

156 g/m^2/yr, making them among the highest reported in the Northern Hemisphere (Muhs et al.
157 2013). Crusius et al. (2011) estimated that a single dust storm in 2006 from the Copper River
158 basin could have delivered 30–200 metric tons of soluble Fe to the GOA. Glaciogenic dust
159 therefore may play an important role in fertilizing the northeastern subarctic Pacific.
160 A detailed understanding of terrestrial micronutrient sources, including their mineralogy,
161 Fe geochemistry, and Fe solubility is needed to help estimate their potential to impact marine
162 phytoplankton communities. This information, in turn, can contribute to an understanding of the
163 role of changing nutrient deposition in declining North Pacific primary production, and the
164 vulnerability (or resilience) of the subarctic Pacific ecosystem to ongoing climate change. In this
165 study we evaluate four classes of terrestrial nutrients in terms of their potential to deliver
166 bioavailable Fe and other trace metals: Asian desert sediment, aged and fresh volcanic ash, and
167 glacier-derived sediment, including glaciofluvial silt and loess. We compare data from a range of
168 well-established protocols, finding that glacially-sourced dust outpaces both volcanic ash and
169 desert dust as a source of bioavailable trace nutrients.
170
171 **2. Materials and Methods**
172
173 **2.1 Sample collection**
174
175 **2.1.1 Glaciofluvial silt and loess samples**
176 We collected glaciofluvial silt and loess samples from southcentral Alaska, USA, in
177 summer 2016 and from Yukon Territory, Canada, in summer 2017 (Fig. 1). Glaciofluvial silts
178 were collected from river channel deposits or river banks downstream from alpine glaciers. We
179 sampled silt from the Chistochina, Copper, Gakona, Knik, Matanuska, and Susitna Rivers, which
180 collectively represent erosion of bedrock from the Alaska, Talkeetna, Chugach, and Wrangell
181 mountain ranges. The Alaska and Yukon samples are considered collectively in subsequent
182 figures and text as "AK glaciofluvial silt." We sampled loess from the Matanuska and Copper
183 River valleys, including a section at the confluence of the Chitina and Copper Rivers described
184 and radiocarbon-dated by Muhs et al. (2013). In total, we analyzed 20 glacier-derived samples,
185 including eleven glaciofluvial and nine loess samples (Table 1).
186

2.1.2 Volcanic ash samples

Volcanic ash samples include two fresh, never-wetted samples from the Redoubt 2009 and Pavlof 2016 eruptions, and six aged ash samples from Redoubt and Augustine volcanoes which represent deposition over the past ~8700 cal years B.P. (Fig. 1). Fresh ash from Redoubt Event 19 erupted on 4 April 2009 (sample AT-3982) was collected in Homer, Alaska (115 km to the SE) as a 1-mm layer on clean poster board. Fresh ash from Pavlof erupted on 28 April 2016 (AT-3680) was collected from wood planks of a porch in Nelson Lagoon (78 km to the NE). One aged ash sample (AT-1411), inferred to be from the 1989–1990 eruption of Redoubt Volcano, was collected from beneath modern leaf litter along the Drift River (11 km NE). Five other aged ash samples (AT-2851, 2854, 2867, 2876, 2886) were collected from a surface pit in a coastal bluff 20 km W of Augustine Island (Fig. 1).

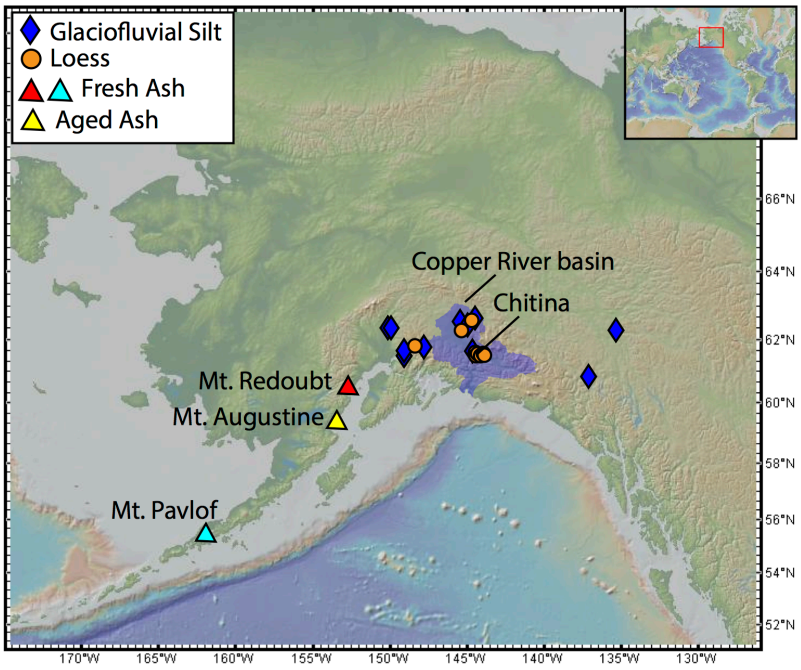

Figure 1. Map showing sample sites in Alaska and the Yukon Territory, including the Chitina loess section and Copper River basin. Map generated using GeoMapApp.

2.2 Sample processing

A summary of the sample processing and analytical methods can be seen in Fig. 2.

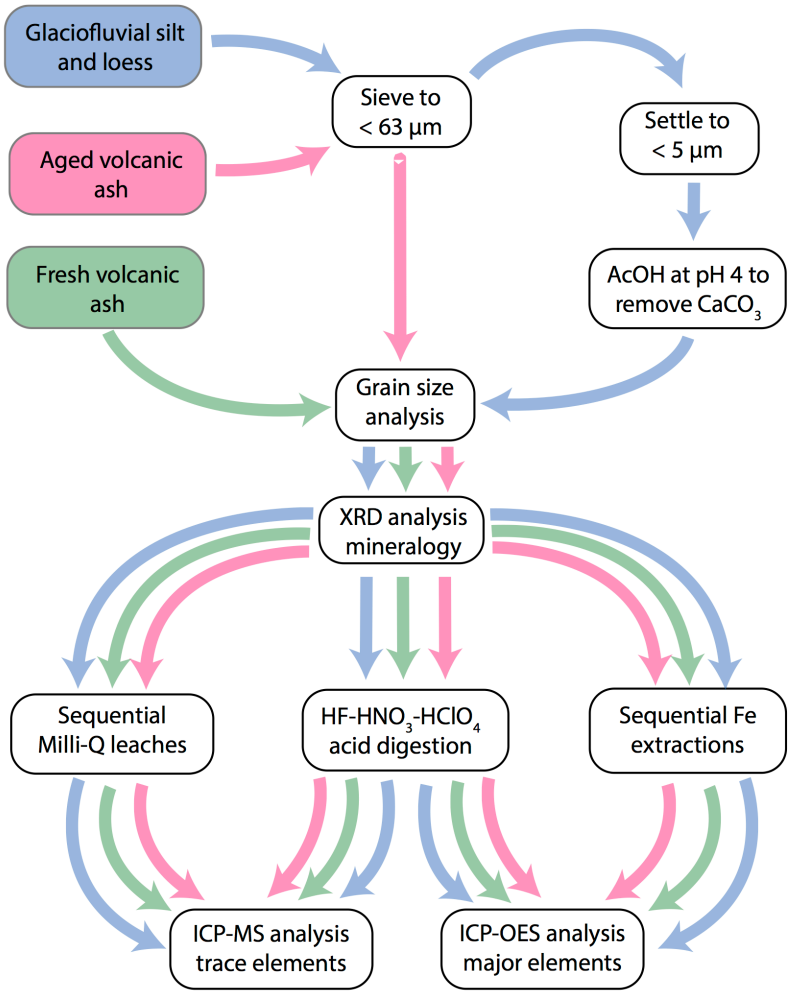

Figure 2. Flowchart diagram showing sample processing and analysis steps used in this study. Not all samples went through all procedures.

2.2.1 Size separation

Glaciofluvial and loess samples were separated by size, first using wet sieving (<63 µm diameter) and then humid sedimentation following Stokes' law (<5 µm diameter), assuming spherical grains. Ultrapure water used for all experiments came from a Milli-Q Integral 3 System. The <5 µm fraction represents the material most likely to be wind-transported (Prospero 1999). It is important to perform analyses specifically on the size fraction that is transported offshore since there may be geochemical and mineralogical variation based on grain size. For example, the Fe content of our <5 µm samples is likely higher in finer grain sizes relative to bulk sediment, as Fe-bearing clay minerals and iron oxides, such as hematite, goethite, and chlorite,

tend to be smaller (Whitney 1975; Poulton and Raiswell 2005; Lu et al. 2017). Grain size separations were not performed on pristine ash samples because we did not want to alter the Fe geochemistry of these never-wetted samples prior to the sequential Fe extractions. Specifically, we were interested in detecting surficial Fe sulfate salts, which we expected would dissolve in the $MgCl_2$ extraction. Aged ash samples were sieved to remove >63 μm material, which was generally negligible. Grain size distributions for all sample types are shown in Fig. 2 and discussed in Section 3.3.

2.2.2 Leaching

Fine-grained (<5 μm diameter) glaciofluvial and loess samples were leached to remove carbonates using a pH 5 buffered acetic acid solution until non-reactive. A visible reaction occurred for loess samples from the Chitina loess section, which contained gastropod shells, but not for other sediment samples.

2.3 Analytical methods

2.3.1 Grain size distribution

We measured grain size distribution using a Beckman Coulter Multisizer 3 with a 100 μm aperture tube and glass propeller stirrer. We used Isoton II diluent in a 50% dilution, running each sample at least 3 times. All labwork was conducted in a new, purpose-built facility at Colby College, which provides the low blanks required for trace-metal clean procedures. The lab has a dedicated air handling system that maintains HEPA filtration and minimum humidity levels. The main laboratory is accessed via an adjacent anteroom where workers don non-particulating lab coats, hair nets, dedicated clogs, and nitrile or vinyl gloves.

Particle blanks were consistently ≤0.5% of sample concentrations, and we did not perform a blank correction. Both concentration and particle sizing measurements were highly reproducible. For example, twelve analyses of a sediment sample gave concentrations with a 1% residual standard deviation (%RSD). Individual size bins with counts per bin of ~10–1500 particles/mL yielded 2*standard errors of ≤ 1 particle/mL in size bins 2–13 μm diameter. In bins greater than 13 μm, the rarity of coarse particles in our samples led to spikier data, and 2*standard errors ranged from 1–7 particle/mL.

246

247 **2.3.2 Fractional solubility via ultrapure water leaches**

248 Iron and other trace metal fractional solubility was determined following the ultrapure
249 water leaching procedure of Schroth et al. (2009). We placed 3–4 mg of sediment (weighed
250 using a Sartorius Cubis Ultra-Microbalance, which has repeatability to +/- 0.00025 mg) on a 0.4-
251 μm-pore Whatman polycarbonate filter in an acid-cleaned Nalgene filter holder. The sediment
252 was leached with Milli-Q™ ultrapure water under vacuum at a rate of 250 mL per 45 seconds.
253 Water was passed through the filter in incremental steps of 100 mL, 150 mL, 250 mL, and 500
254 mL, for a total volume of 1000 mL, to assess progressive solubility. Each sample was leached in
255 triplicate and acidified to 3% v/v nitric acid prior to analysis. Procedural blank concentrations
256 represented 6–30% of the sample concentrations, and blank corrections were performed.
257 We recognize that ultrapure water itself bears little resemblance to seawater and real-
258 world conditions. However, this simple and widely-used experimental design allows for the
259 evaluation of relative differences among sample types and between studies (e.g, Shelley et al.
260 2018). We also note that any measure of solubility is operationally defined and may reflect some
261 combination of dissolved and colloidal Fe (Wu et al. 2001).

262

263 **2.3.3 Sequential Fe extraction**

264 Iron has varying chemical reactivity and solubility based on how it is bonded within
265 minerals and other compounds. Sequential Fe extractions aim to remove and analyze Fe
266 contained as: 1) exchangeable Fe(II) ions (including iron-bearing salts), 2) "easily-reducible" Fe
267 oxides (ferrihydrite and lepidocrocite), 3) "reducible" Fe oxides (goethite, hematite, and
268 akaganéite), and 4) Fe (oxyhydr)oxides as well as Fe from sheet silicates (e.g., chlorite and
269 biotite) (Chester and Hughes 1967; Poulton and Canfield 2007; Lu et al. 2017; Slotznick et al.
270 2019). While each extractant targets a specific group of minerals, it is not mineral-specific, and
271 minerals may dissolve across multiple extraction steps (Slotznick et al. 2019). However, the
272 extractions provide useful operational definitions for comparisons among sample types.
273 Beginning with 100 mg of sediment in a 15 mL centrifuge tube, each extractant was
274 added, sonicated and vortexed until sediment became fully suspended. After each extraction,
275 samples were centrifuged for twenty minutes at 3900 RPM and the supernatant was collected for
276 analysis. The first extraction uses 10 mL of 1 M magnesium chloride, brought to pH 7 with 1 M

277 sodium hydroxide and rocked for two hours, to extract exchangeable Fe(II) ions (Heron et al.
278 1994; Poulton and Canfield 2005). For the second extraction, we added 10 mL of 1 M
279 hydroxylamine–hydrochloride solution in 25% v/v acetic acid to each sample, then placed
280 samples on a rocking table for 24 hours under dark conditions to extract easily-reducible Fe
281 oxides (Chester and Hughes 1967; Poulton and Canfield 2005). The third extraction adds 10 mL
282 of sodium dithionite solution (50 g/L, buffered to pH 4.8 with acetic acid, sodium citrate, and
283 sodium bicarbonate) to each sample. These were placed in an 80˚ C water bath for 30 minutes
284 and shaken every five minutes, to extract reducible Fe oxides (Mehra and Jackson 1958; Poulton
285 and Canfield 2005; Lu et al. 2017). This extraction has been found to be the "most robust at
286 extracting the targeted phases" (Slotznick et al. 2019). We then added 3 mL of 6 N HCl at 100˚C
287 in Teflon beakers for 2 hours for the final extraction of Fe (oxyhydr)oxides and Fe from sheet
288 silicates (Poulton and Canfield 2005; Lu et al. 2017). Following this step, we performed an HF-
289 HNO_3 hotplate digestion following the procedure described in section 2.3.4 to determine residual
290 iron concentrations (results discussed in section 3.4).
291
292 **2.3.4 Hotplate digestion**
293 To digest the samples, we weighed 100 mg of sample into Savillex™ beakers, then added
294 concentrated in-house double-distilled HNO_3 and Seastar® Ultrapure HF in a 3:1 ratio. Samples
295 were disaggregated in an ultrasonic bath for 20 minutes and heated, capped, at 100°C for >24
296 hours. Some glaciofluvial silt and loess samples contained organic carbon, appearing as a black
297 residue. These required the addition of 0.3–0.5 mL concentrated Fisher Chemical Optima $HClO_4$,
298 followed by fuming at 200°C in a dedicated hood with washdown system. We repeated this step
299 until the samples dried to whitish cakes. Residual halides were removed by two successive
300 additions of 6 mL double-distilled 8N HNO_3 followed by 20 minutes in an ultrasonic bath and
301 >1 hour heating, capped, at 100°C. Dried, digested samples were brought up to 5 mL in 4N
302 HNO_3. Rock standard BCR-2 was digested and processed in parallel with each batch of samples
303 to ensure analytical accuracy (Jweda et al., 2015), and a procedural blank accompanied each
304 batch of samples through all steps. Digestions were performed in laminar-flow exhausting hoods
305 in a clean lab (described in Section 2.3.1).
306
307 **2.3.5 Major and trace element analysis**

Major element concentrations in digested and extracted samples were determined using a Spectro Arcos ICP-AES housed at Colby College. USGS rock standards AGV-2, SCO-1, SDC-1, and BCR-2 were used as a calibration curve to find sample major oxide weight percentages. Trace element concentrations and Fe concentrations from the solubility experiments were measured on a Thermo Finnigan Element II high-resolution ICP-MS at the University of Maine. ICP-MS samples were run using an Elemental Scientific PFA-ST self-aspirating nebulizer with 100 µL/min uptake and a quartz cyclonic spray chamber. Sample gas flow was ~0.8mL/min with additional gas of ~0.2mL/min and RF power of ~1280. All settings were optimized during tuning before analyzing samples. We determined trace element concentrations by analyzing a mixed-matrix elemental standard at four dilutions spanning the expected concentrations of our samples. A check standard was analyzed periodically to assess for analytical drift. USGS rock standards BCR-2, AGV-2, SDC-1, and SCO-1 were run as "random" samples on the ICP-MS to assess accuracy. Procedural blank concentrations were negligible, and no blank corrections were performed. We calculate percent residual standard deviation (%RSD) using data from six independent digestions and seven independent analyses of BCR-2. We find %RSDs <8% for all elements except Co, As, Ag, and Cd, which are among the lowest-concentration elements for BCR-2.

2.3.6 X-Ray diffraction

The mineralogy of samples was determined at Colby College using a Bruker D2 Powder Phaser X-ray diffractometer (XRD) with a Cu Kα anode and goniometer radius of 141.00 mm. The <5µm grain size fraction of sediment samples was analyzed; bulk samples were used for the volcanic ash samples. Approximately 15 mg of sample was suspended in Milli-Q water, pipetted onto a silica zero-background wafer, and dried down to align clay minerals. Samples were analyzed for 2$\boldsymbol{\theta}$ values from 5–30˚ with a step size of 0.020˚. Peaks were identified using Bruker Diffrac.EVA software with International Center for Diffraction Data PDF-4+ 2019 database and compared to those documented in the literature (Moore and Reynolds 1989; Lu et al. 2017; Muhs et al. 2013).

2.3.7 Radiocarbon dating of aged ash samples

Ages of ash samples collected from the soil pit near Augustine Island were determined by radiocarbon dating of the humic acid fraction of underlying soils. Samples were processed either at the USGS AMS Radiocarbon Lab in Reston, VA with analysis at the Center for Mass Spectrometry, Lawrence Livermore National Laboratory in Berkeley, CA, or at the University of Georgia Center for Applied Isotope Studies in Athens, GA (Table 2). Raw ages were calibrated using CALIB v.5 (Stuiver and Reimer, 1993) and 95% age distributions at 2σ were found using IntCal04 (Reimer et al., 2004).

3 Results

3.1 Grain size distribution

Sediments subjected to sieving and settling for grain size separation had approximately lognormal volume distributions (dV/dlnD), with volume mode diameters of ~4–4.5 µm (Fig. 3). Fresh and aged ash samples, which were run as bulk and <63 µm size fractions, respectively, had coarser grain size distributions. The fresh ash sample we analyzed in duplicate, AT-3982, had a volume mode diameter of ~10–11 µm. Two aged ash samples, AT-2876 and AT-2886, had volume mode diameters of ~20 µm (Fig. 3).

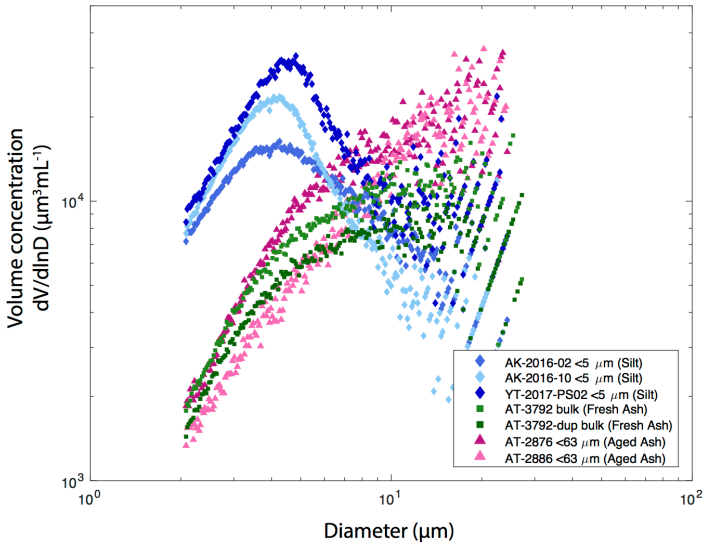

Figure 3. Particle volume size distributions (dV/dlnD). Size-separated sediments have volume mode diameters of ~4–4.5 µm, while pristine ash samples, which were not size-separated, have volume mode diameters of ~10–11 µm. Aged ash samples are a bit coarser, with mode diameters of ~20 µm.

3.2 Fe content and solubility of dust and ash

The total Fe content of the bulk fresh ash samples from Redoubt (AT-3982) and Pavlof (AT-3680) were 5.96 wt % and 11.9 wt % respectively. Aged ash samples from Redoubt and Augustine ranged from 4.49 wt % to 7.06 wt %, with a median of 4.97 wt %. The total Fe

content of the <5 µm glacier-derived sediments ranged from 6.89 to 14.1 wt % with a median of 10.6 wt %. Glacier-derived Alaska sediments had greater total Fe content than the Asian desert samples analyzed by Lu et al. (2017); the average Fe concentrations from each desert ranged from 5.92 ± 1.41 wt % (n = 5; 1 s.d.) to 8.38 ± 1.55 wt % (n = 37; 1 s.d.) Fe, with a median of 6.92 wt % (Lu et al., 2017).

Glaciofluvial silt, loess, and aged ash samples had similar cumulative fractional Fe solubility ($\%Fe_S$) values after leaching with 1000 mL of ultrapure water, ranging from 0.12% to 0.76%, with a median solubility of 0.32% (Table 3). There were no significant differences among these three sample types (Fig. 4). In contrast, the two fresh ash samples had significantly lower cumulative Fe solubilities, at 0.06% and 0.03% (Fig. 4). In all samples, Fe solubility was positively associated with easily-reducible Fe content (r = 0.33) and Fe contained in sheet silicates and (oxyhydr)oxides (r = 0.31), and negatively associated with the residual Fe fraction (r = -0.49).

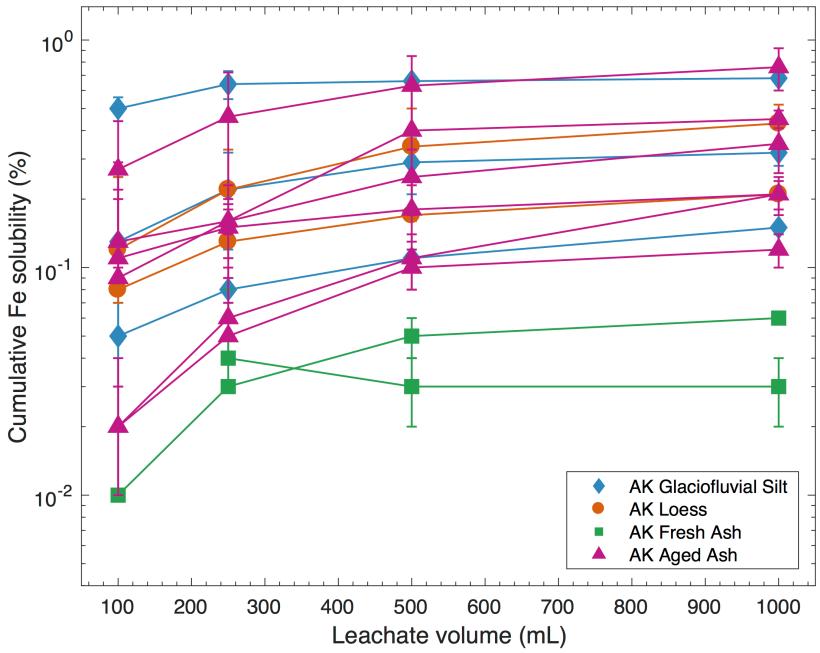

Figure 4. Cumulative fractional Fe solubility following successive leaches of sediment/ash samples with Milli-Q water. Fresh volcanic ash samples are ~7x less soluble than aged ash, loess, and glaciofluvial silt samples (calculated using median values), which all have similar Fe solubility. Samples were leached in triplicate, and error bars represent one standard deviation.

3.3 Trace metal (Mn, Co, Ni, Cu, Zn, Mo, Cd, Pb) content and solubility of dust and ash

Bioactive and/or potentially toxic trace metal concentrations were generally higher in glacier-derived sediments than in ash samples (Table 1). Most of these metals followed one of two patterns. For Ni, Cu, and Pb, concentrations in silt and loess were similar, and were 5–30

times higher than in fresh or aged ash samples, which were similar to each other (Fig. 5A-C). Specifically, Ni concentrations followed the order: silt (median: 89.4 ± 22.3 ppm median absolute deviation (MAD); n = 11), loess (84.7 ± 34.4 ppm; n = 8), aged ash (8.2 ± 5.8 ppm; n = 6), fresh ash (2.9 ± 1.0 ppm; n = 2). Cu concentrations were: loess (209 ± 81.2 ppm), silt (158 ± 30.9 ppm), fresh ash (39.4 ± 1.5 ppm), aged ash (37.2 ± 14.4 ppm). Pb concentrations followed the order: silt (30.2 ± 4.1 ppm), loess (30.1 ± 12.7 ppm), fresh ash (5.9 ± 1.0 ppm), aged ash (5.2 ± 2.7 ppm). For Co, Zn, Mo, and Cd, silt samples had the highest concentrations, but the four sample types were much closer in value, with more overlap in their ranges (Fig. 5D-G). Specifically, Co concentrations were: silt (38.0 ± 5.1 ppm), loess (26.9 ± 10.4 ppm), fresh ash (15.5 ± 4.3 ppm), aged ash (11.5 ± 2.9 ppm). Zn concentrations decreased in the order: silt (249 ± 47.7 ppm), loess (118 ± 7.6 ppm), fresh ash (100 ± 12.4 ppm), aged ash (73.9 ± 19.8 ppm). Mo concentrations were: silt (3.2 ± 1.4 ppm), loess (2.9 ± 1.8 ppm), aged ash (2.4 ± 0.6 ppm), fresh ash (1.3 ± 0.2 ppm). Cd concentrations were quite low, with: silt (0.19 ± 0.05 ppm), loess (0.14 ± 0.05 ppm), fresh ash (0.11 ± 0.02 ppm), aged ash (0.07 ± 0.02 ppm). Mn concentrations were highest in fresh ash (611 ± 161 ppm) and silt (547 ± 193 ppm), and lower in aged ash (338 ± 48 ppm) and loess (306 ± 113 ppm) (Fig. 5H).

We determined the cumulative fractional solubility of Mn, Cu, and Co following leaching with 1000 mL of Milli-Q water (see section 2.3.2), and found that values were similar among sample types (Table 3). Cu solubilities were highest (median: 4.4 ± 3.4% MAD; n = 10), followed by Mn (1.6 ± 1.1%; n = 13) and Co (0.8 ± 0.2; n = 13). For the other metals, concentrations were either below detection limits, or had higher blanks, likely because of contributions from the filters, and thus we were unable to determine fractional solubilities using this approach.

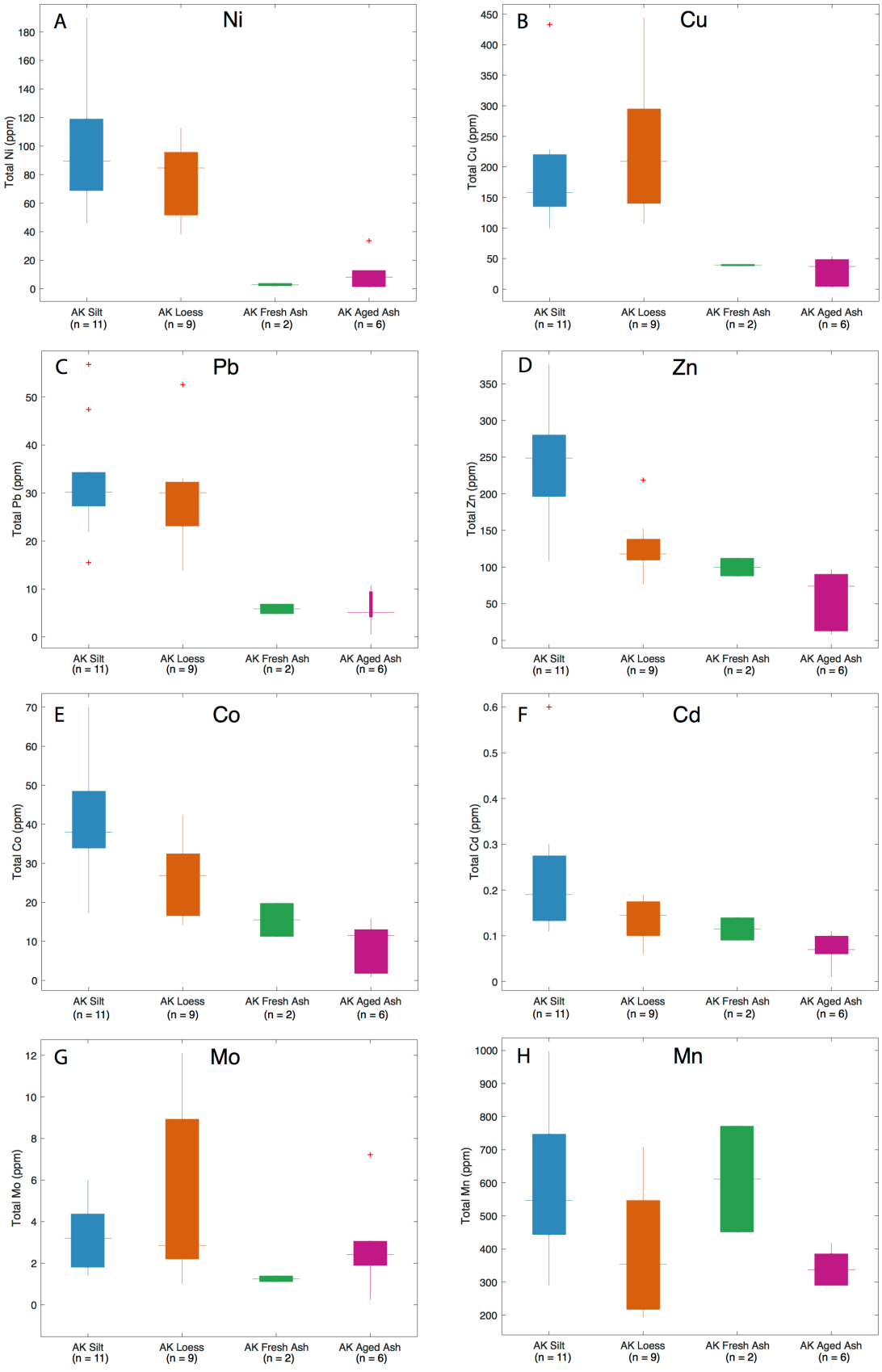
A
Ni
Total Ni (ppm)
B
Cu
Total Cu (ppm)
C
Pb
Total Pb (ppm)
D
Zn
Total Zn (ppm)
E
Co
Total Co (ppm)
F
Cd
Total Cd (ppm)
G
Mo
Total Mo (ppm)
H
Mn
Total Mn (ppm)
AK Silt (n = 11)
AK Loess (n = 9)
AK Fresh Ash (n = 2)
AK Aged Ash (n = 6)

401

Figure 5. Box-and-whisker plots showing concentrations of bioactive and/or potentially toxic trace metals among four sample types. Boxes represent 25th and 75th percentiles, while the thin horizontal line shows the median value of each dataset. Whiskers (thin vertical lines) indicate the data range, excluding statistical outliers (outside ~2.7σ). Trace metals generally follow one of two patterns: Ni (A), Cu (B), and Pb (C) are 5–30x higher in loess and silt samples than in ash samples. Concentrations of Zn (D), Co (E), Cd (F), and Mo (G) are much more similar among samples, though glacier-derived samples remain higher than ashes. Mn (H) is slightly higher in fresh volcanic ash samples than in silt samples, while loess and aged ash have lower but similar concentrations.

3.4 Fe speciation

Glaciogenic sediments, including silt and loess, had the highest weight percentage of easily-reducible Fe (median: 2.3 ± 0.6 MAD; n = 20), nearly five times higher than Asian desert sediments (0.49 ± 0.1 wt %; n = 108; data from Lu et al., 2017) and fourteen times higher than fresh volcanic ash (0.16 ± 0.1 wt %; n = 2) (Fig. 6; Table 4). There were no significant differences in the easily-reducible Fe content of silt vs. loess samples. Proportionally, easily-reducible Fe made up 23 ± 7.5% of the total iron in the glacier-derived samples compared to 7.8 ± 1.6% in Asian desert sediments and 1.7 ± 0.2% in fresh ash. Aged volcanic ash contained 1.6 ± 0.3 wt % (n = 6) easily-reducible Fe, ten times higher than fresh ash. Easily-reducible Fe accounted for 33 ± 2.2% of the total Fe in aged ash, twenty times higher than its proportion in fresh ash. Fig. 6 provides a summary of the Fe extraction data among sample types, shown as proportions of total Fe. We use estimation plots to illustrate the differences among sample types (Fig. 7A) (Ho et al., 2019). These provide the distributions of values as well as the average difference (with 95% confidence interval) between each sample type and a reference data set, in this case, Asian desert sediment (from Lu et al., 2017).

Reducible Fe oxides were most abundant in Asian desert sediments, at 2.4 ± 0.42 wt %, equivalent to nine to 172 times higher than in other sample types. By comparison, glaciogenic sediments contained 0.18 ± 0.07 wt % reducible Fe; fresh ash contained 0.014 ± 0.002 wt % reducible Fe, and aged ash contained 0.27 ± 0.05 wt % reducible Fe. Proportionally, reducible Fe accounted for 34 ± 3.3% of the Fe in Asian sediments, whereas it comprised 1.6 ± 0.55% of the Fe in glaciogenic sediments, 0.18 ± 0.08% of the Fe in fresh ash, and 5.6 ± 0.72% of the Fe in aged ash (Figs. 6, 7B). Among the glaciogenic samples, loesses had higher and more variable concentrations of reducible Fe oxides (0.74 ± 0.56 wt %) than silts (0.14 ± 0.05 wt %).

Exchangeable Fe(II) ions were negligible in most samples, but three AK loess samples had ~1% of their total Fe in this form.

Glaciogenic samples had the highest concentrations of Fe as sheet silicates and (oxyhydr)oxides, at 6.8 ± 1.0 wt %, making them 2–3x higher than fresh ash (2.7 ± 0.39 wt %), aged ash (2.4 ± 0.51 wt %), and Asian desert sediments (3.2 ± 0.23 wt %). Silts had higher and less variable concentrations (6.9 ± 0.81 wt %) than loess samples (5.0 ± 3.3 wt %). Proportionally, glaciogenic sediments contained 62.4 ± 9.3% of their Fe in this form, compared to 34.7 ± 15.3% in fresh ash, 45.8 ± 7.6% in aged ash, and 43.4 ± 4.2 % in Asian desert sediment (Figs. 6, 7C).

As determined following complete acid digestion of the remaining sediment after the first four extractions, fresh ash samples contained by far the highest refractory Fe, at 6.2 ± 3.2 wt %. In comparison, other sample types contained close to 1 wt % refractory Fe. Proportionally, refractory Fe accounts for 63.2 ± 15.3% of the Fe in volcanic ash, compared to 22.9 ± 2.9% of Fe in aged ash, 12.4 ± 3.0% of Fe in Asian desert sediment, and 9.8 ± 2.1% of Fe in glaciogenic sediments (Figs. 6, 7D). Of the samples analyzed here, freshly deposited volcanic ash contained the least Fe in a form potentially usable by phytoplankton, and the most Fe in a refractory form.

The sum of extracted Fe compares reasonably well to the total amount of digested Fe measured in each sample, with extracted Fe representing 73 to 109% of digested Fe (mean: 95.8% ± 10 s.d.) (Fig. 8). Differences may relate to errors in sample weights or to different analytical runs. In comparison, the percentage of extracted Fe from Asian desert sediments relative to total Fe ranges from 81 to 128% (Lu et al. 2017). The Asian desert dust values fit the 1:1 line more closely than the Alaska and Yukon samples, likely because each point represents an average of samples from each desert region.

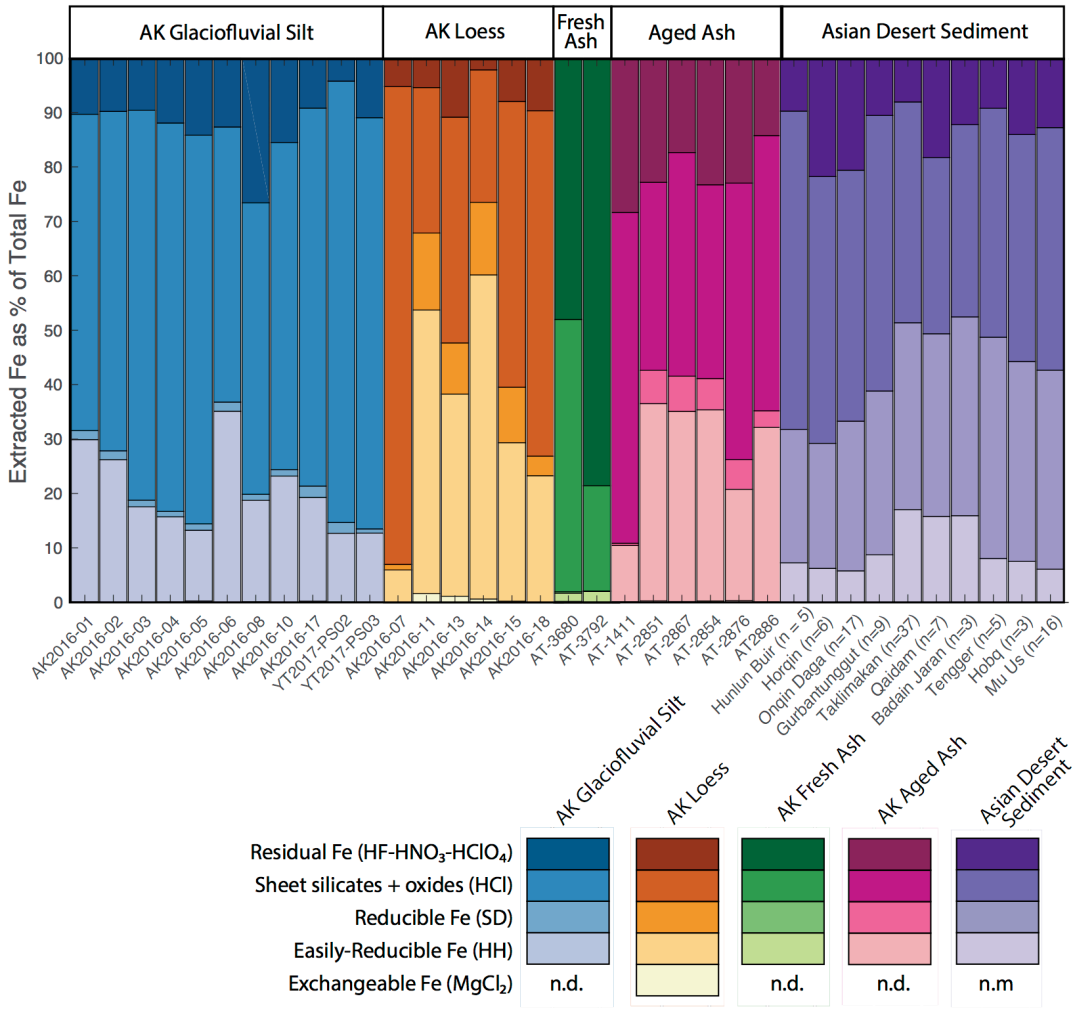

Figure 6. Stacked bar plot showing proportions of total Fe represented by each Fe extractant. Color hues represent sample type, with tints indicating the Fe extraction used (see legend). Asian desert sediment bars represent means of samples from each desert (numbers given in parentheses) (Lu et al., 2017). Glaciofluvial silt, loess and aged ash samples have the highest proportions of easily-reducible Fe, while Asian sediments have the highest proportion of Fe as reducible Fe oxides. The majority of Fe in fresh volcanic ash samples is refractory.

3.5 Mineralogy

Chlorite, muscovite, quartz, and plagioclase were the dominant mineral phases present in the glacier-derived silt and loess samples (Fig. 9). Chlorite was the most abundant Fe-bearing mineral and one of the most abundant minerals present; prominent (002) and (004) peaks relative to (001) and (003) peaks suggest that it is Fe-rich (Muhs et al., 2013). We did not detect iron oxide minerals in these samples using XRD, although from the sequential Fe extraction results, we infer the presence of easily-reducible Fe oxides such as ferrihydrite, and reducible Fe oxides

such as hematite and goethite. Pristine ash samples contain quartz, plagioclase, and muscovite, though presumably are largely non-crystalline, with Fe occurring in the glass both in the interstices between silica tetrahedra, and substituting for Si^{4+} within tetrahedra (Ayris and Delmelle, 2012).

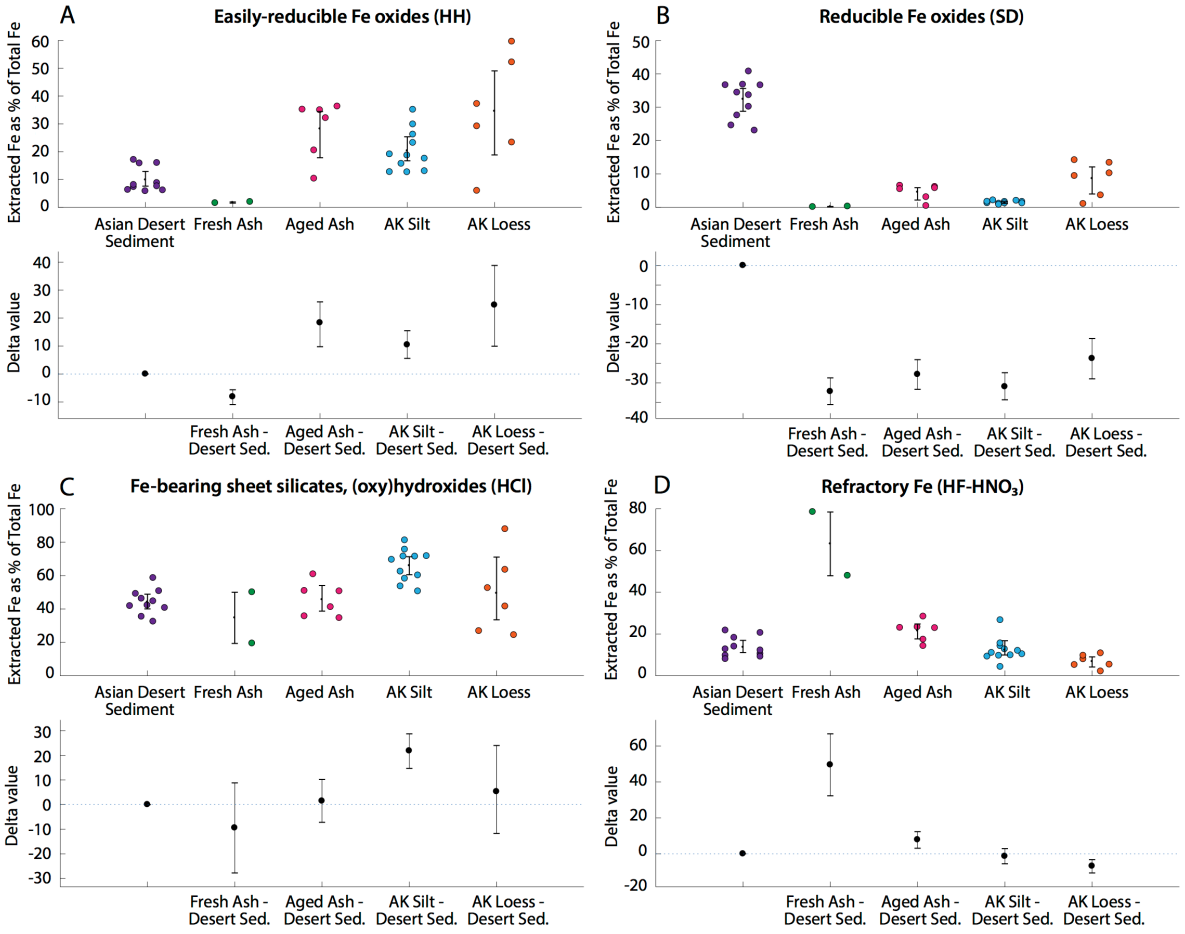

Figure 7. Estimation plots of sequential Fe extraction data after Ho et al. (2019). Upper panels show distributions of values as % of total Fe represented by each extractant, with error bars giving the mean (black dot) and one standard deviation of each dataset. Lower panels show the average difference between each sample type and Asian desert sediment (from Lu et al., 2017). Error bars give 95% confidence intervals of the delta values. A) Fresh ash samples have lower easily-reducible Fe than Asian desert sediments, while aged ash, silt, and loess samples have ~3x higher easily-reducible Fe than desert sediments. B) Asian desert sediments have the highest proportion of reducible Fe oxides, ~3x higher than Alaska ash and sediment samples. C) Glaciofluvial silt samples have 2x higher proportions of Fe contained as sheet silicates and (oxy)hydroxides than Asian desert sediments and fresh and aged ashes. D) Fresh volcanic ash has ~3x higher refractory Fe than other sample types. Exchangeable Fe ($MgCl_2$ extraction) data are not shown, as this fraction was only detected in three loess samples.

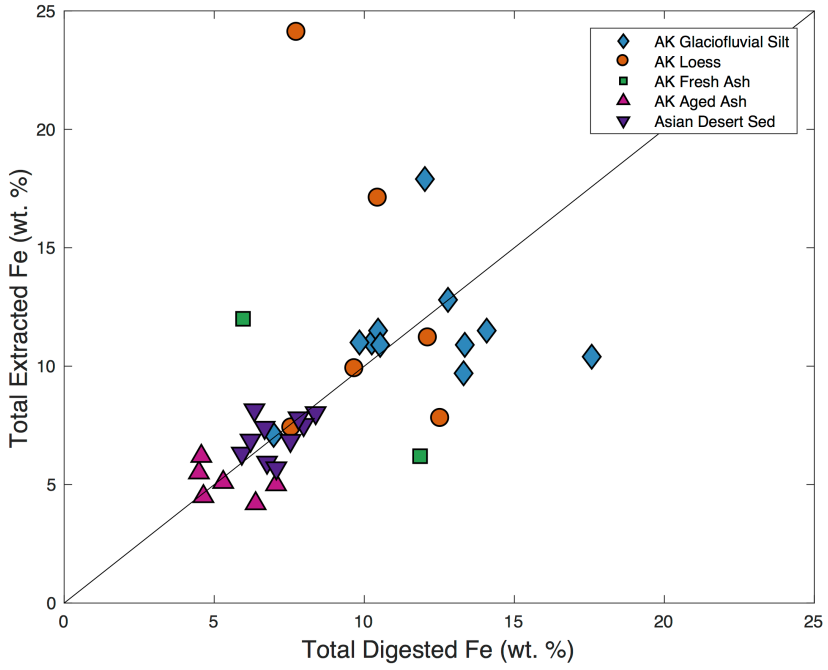

Figure 8. Comparison of total extracted Fe to total digested Fe for independently processed and analyzed samples measured in this study and Asian desert sediments analyzed by Lu et al. (2017). Most samples fall near the 1:1 line, though several are significantly different between the two approaches.

490

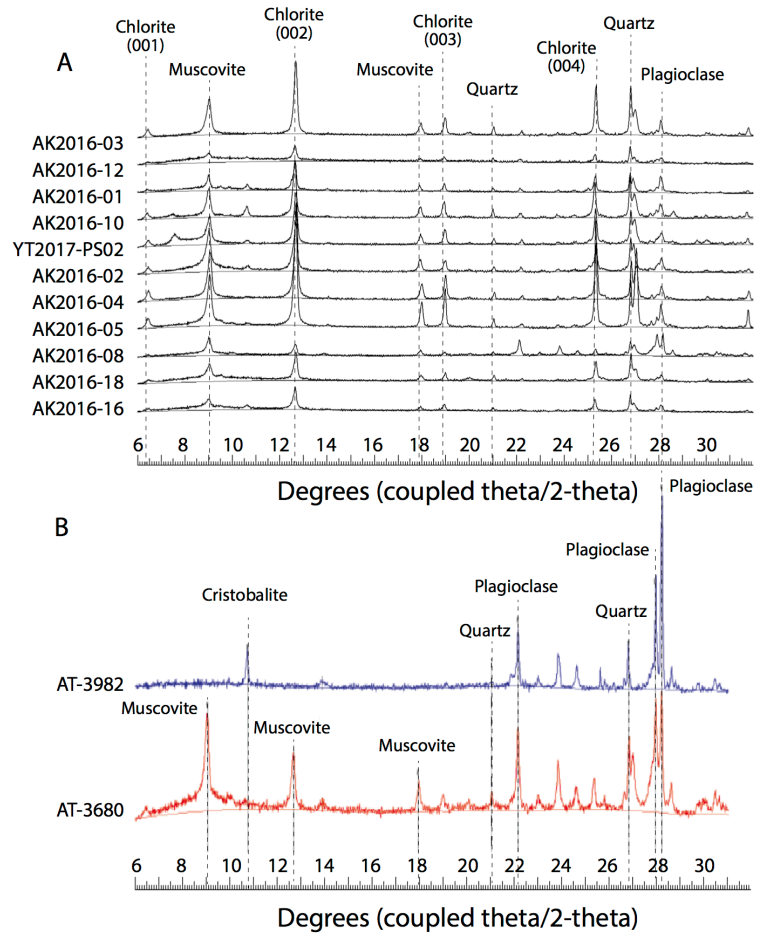

Figure 9. Representative XRD spectra showing mineralogy of A) glacier-derived silt and loess samples and B) fresh volcanic ash samples. Chlorite appears as the dominant Fe-bearing mineral in glacier-derived samples, while ash samples do not contain any obvious Fe-bearing minerals.

491

4 Discussion

4.1 Fe geochemistry, solubility, and mineralogy

We observed several key differences in the Fe geochemistry of glacier-derived and Asian desert sediments, hinting at differences in their potential impacts on ocean ecosystems. Glaciogenic silt and loess samples contained more Fe (median = 10.6 wt %) than the Asian sediment samples (median = 6.92 wt %) characterized by Lu et al. 2017 (Table 1), suggesting that even if there were no differences in the speciation or solubility of iron, glacier-derived dust would provide the northeastern subarctic Pacific more Fe per unit mass than would Asian dust. Reported values of bedrock from southcentral Alaska, where the silt and loess were collected, range from 2.38 to 17.0 wt % with a median of 8.68 wt % (Greene et al. 2006, found on www.earthchem.org/petdb). Since the median sediment concentrations are higher in the fine-fraction material, it may indicate that there is an enhancement of Fe in the <5 μm grain size fraction relative to the bedrock, perhaps related to Fe-bearing clays (Journet et al. 2008).

While total Fe contents between Alaska and Asian samples differ, we also see significant differences in the speciation and solubility of glacier-derived vs. desert-derived dust. Glacier-derived samples, including glaciofluvial silt and loess, have the highest weight percentages of easily-reducible iron, five times higher than Asian desert sediments and fourteen times higher than fresh volcanic ash. They also have twice as high Fe extracted from sheet silicates than either ash or Asian desert sediments. XRD analysis shows that chlorite is a dominant Fe-bearing mineral (and sheet silicate) in these samples, and we also infer the presence of Fe oxides such as ferrihydrite and goethite, based on the sequential Fe extraction data (e.g., Slotznick et al., 2019). Overall, the silicate mineralogy of the sediment samples is dominated by chlorite, muscovite, quartz, and plagioclase. In comparison, fine-grained Asian desert sediments are, on average, dominated by secondary minerals including illite (55%), kaolinite (29%), chlorite (12%) and smectite (4%), with ~2% hematite and goethite (Lu et al. 2017). Overall, Asian desert sediments have lower proportions of Fe as sheet silicates and higher proportions of Fe as reducible Fe oxides (hematite and goethite) than Alaska glacier-derived sediments (Figs. 6-7). These differences exist despite the fact that Lu et al. (2017) analyzed the <2 μm fraction, while our sediments are coarser, with ~5 um diameter (Fig. 3).

523 Mineralogical results from Alaska are broadly consistent with those of Muhs et al.
524 (2013), who analyzed the bulk and <53 μm fractions of loess samples from two of the same sites
525 analyzed in this study: Chitina and Matanuska valley, Alaska. Muhs et al. (2013) identified
526 quartz, plagioclase, amphibole, and chlorite, with lesser amounts of K-feldspar, mica, and
527 carbonate minerals. We did not detect amphibole or K-feldspar, and removed carbonates through
528 an acetic acid leach prior to analysis. We also see some broad similarities to the findings of
529 Schroth et al. (2009), who used EXAFS spectra to infer the dominant minerals within Asian and
530 Alaska sediments. Namely, there is a significant contribution of Fe oxides in Asian desert
531 samples and of primary silicates in Alaska glaciofluvial samples (Schroth et al., 2009, 2011).
532 However, there are some differences: Schroth et al. (2009) identified only ferrihydrite and
533 hornblende in an Asian desert sample, whereas Lu et al. (2017) measured a range of clay
534 minerals and Fe oxides, with Fe contributions from chlorite, hematite, and goethite. Schroth et al.
535 (2009) inferred large fractions of biotite, hornblende, ferrosmectite, and ferrihydrite in Alaska
536 sediments, whereas both Muhs et al (2013) and this study identified chlorite as a dominant Fe-
537 bearing mineral. These differences probably can be attributed to the different instrumentation
538 and associated procedures used to identify minerals, as well as differences among samples.
539 Fe solubility results are consistent with the sequential extraction and mineralogy data,
540 showing relatively high cumulative Fe solubility of 0.12% to 0.76% in silt and loess samples
541 following leaching with 1000 mL of ultrapure water, but much lower values of 0.03% and 0.06%
542 in fresh volcanic ash. Results are consistent with previously published data on sediments from
543 glacially-fed rivers obtained using the same experimental setup. Schroth et al. (2009) measured
544 Fe solubility after leaching with 750 mL of ultrapure water, finding values of 0.4% and 0.8%,
545 respectively, in two Alaska glaciofluvial samples. Additional leaching of the same samples with
546 5 L of water yielded higher values of 2–3% (Schroth et al., 2009). Although we did not perform
547 this more extensive set of leaches, we would expect comparable increases in our samples. The
548 volcanic ash solubility results (0.03–0.06% Fe_S) fall near the middle of a previously reported
549 range of Fe_S for fresh volcanic ash samples of 0.007–0.1% Fe_S (Olgun et al. 2011). Overall, our
550 measured values are on the low end of a spectrum of %Fe_S values measured globally, consistent
551 with natural aerosol sources and no input of combustion aerosols (Sholkovitz et al, 2012).
552 Although we expected to measure Fe-bearing salts in the fresh ash samples via the $MgCl_2$
553 extraction, which removes exchangeable Fe(II) ions, we found only negligible amounts of Fe in

554 this form. Though Fe-bearing salts may be present on the ash particle surfaces (Browning et al.,
555 2015), they would account for such a low fraction of the total iron content of the ash (<< 1%),
556 that they would not compensate for the lack of easily-reducible and reducible iron in the ash
557 samples. A second potential source of highly soluble Fe is the formation of ferrihydrite
558 nanoparticles through cloud processing (Shi et al., 2009), which may occur on ash particles
559 (Ayris and Delmelle, 2012). The sequential extraction data show very low percentages of easily-
560 reducible Fe, a pool which includes ferrihydrite. Thus, in these samples we find little evidence
561 for the Fe-bearing compounds thought to play a role in ash Fe solubility. Overall, our results
562 show that fresh volcanic ash has the least Fe fertilization potential of the terrestrial nutrient
563 sources measured.
564 The aged ash samples, in contrast, had fractional Fe solubilities very similar to those of
565 glacier-derived samples (Fig. 4): median of 0.28 ± 0.12% MAD (n = 6) for the aged ashes
566 compared to 0.32 ± 0.11% (n = 5) for the glacier-derived sediments. Although eruptive ash
567 compositions presumably would differ among the volcanoes (Pavlof, Augustine, and Redoubt)
568 and individual events sampled, the difference in Fe_S between the fresh (AT-3982) and aged (AT-
569 1411) samples from Redoubt suggests that geochemical transformations may increase Fe_S as ash
570 ages. The fresh sample (2009 eruption) had Fe_S of 0.06%, while the aged sample (1989 eruption)
571 had Fe_S of 0.35%. The mode particle size of the aged ash samples was slightly coarser than that
572 of the fresh ashes, so these differences cannot be attributed to differences in surface area-to-
573 volume ratios (e.g. Ayris and Delmelle, 2012). We explore additional evidence for time-
574 dependent changes in Fe geochemistry and potential bioavailability in section 4.4.
575
576 **4.2 Trace metal (Mn, Co, Ni, Cu, Zn, Mo, Cd, Pb) geochemistry and solubility**
577 With the exception of Mn, trace metal concentrations were highest in glacier-derived
578 samples (silt and loess), and lowest in ash samples (both fresh and aged) (Fig. 5). The differences
579 were most extreme for Ni, Cu, and Pb, which were five to thirty times higher in the sediments.
580 This pattern is consistent with the Fe geochemistry results; namely, that Fe solubility and the
581 extracted Fe fractions thought to be most available to phytoplankton were higher in the glacier-
582 derived samples than in the fresh volcanic ash samples. Thus, on a per-mass basis, local
583 sediments have greater potential to deliver key trace nutrients to the northeastern subarctic

Pacific than do local volcanoes. Unfortunately, a lack of comparable data on digested fine-fraction sediments from Asian deserts limits the ability to compare trace metal concentrations.

While total metal concentrations may be useful for making basic comparisons among aerosol sources, metal fractional solubility can provide a more realistic estimate of potential release into the surface ocean. Trace metal fractional solubilities are highly dependent on pH, with solubility generally increasing significantly as pH decreases (e.g., Lim et al., 1994). Our values, measured at pH ~5.5, may be most comparable to wet deposition of natural aerosols into the surface ocean, although there are key differences between ultrapure water and rainwater, such as negligible buffering capacity and a lack of natural ligands (e.g., Shelley et al., 2018). Another difference is the length of contact time, as our measurements represent instantaneous solubilities of source sediments, whereas wet-deposited aerosols over the ocean likely have experienced a great deal more processing at acidic pH during transport (e.g., Duce and Tindale, 1991; Cwiertny et al., 2008; Solmon et al., 2009; Chen and Grassian, 2013; Jickells et al., 2016). There may also be a contribution of soluble metals from combustion aerosols in open-ocean locations (Sedwick et al., 2007; Sholkovitz et al., 2012).

We measured cumulative median solubilities of Cu: 4.3 ± 3.9% MAD (n = 11), Mn: 1.6 ± 1.1% MAD (n = 13) and Co: 0.8 ± 0.2% MAD (n = 13), following leaching with 1000 mL of ultrapure water, without finding significant differences between glacier-derived and ash samples. Our measured Mn solubility is generally lower than values reported by other studies that used similar methods. For example, Chance et al. (2015) measured aerosol solubility in the SE Atlantic using a pH 4.7 ammonium acetate leach, and found that Mn solubility ranged from ~12–82%, with a median of ~20%, higher than our measured value. Mn solubility of aerosols collected in the North Atlantic on three GEOTRACES cruises, determined using ultrapure water, was also higher, at 32 ± 13% (Shelley et al., 2018). Saharan aerosols leached with pH 4.7 ammonium acetate and North Pacific aerosols leached with ultrapure water both measured 45% soluble Mn (Buck et al., 2013; Baker et al., 2020). It seems clear that our values, measured directly on dust source sediments or volcanic ash samples near their source, represent something fundamentally different from these open-ocean atmospheric aerosols. Atmospheric processing could play a role in these observed differences, as aerosols over the ocean have experienced at least some degree of processing. An alternative explanation is that high Mn solubilities reflect contributions from Mn oxide coatings on soil particles, which are prevalent in arid regions

(Jickells et al., 2016; Baker et al., 2020 and refs therein). As our samples come from a maritime climate, this may be a better explanation for the observed differences in Mn solubility.

In the case of Co, solubility in southeastern Atlantic aerosols was 2 ± 1%, closer to our median value (0.8 ± 0.2%). In the North Atlantic, Co fractional solubilities spanned a wide range from ~0–100%, with most samples falling between 10–20% (Shelley et al., 2018). A study which leached Cape Verde soil particles with seawater in a flow-through reactor measured fractional Co solubility of 0.14%, bracketing our sample on the low end (Thuroczy et al., 2010). For Cu, our values (4.3 ± 3.9%) are within the range reported for Saharan dust aerosols, 1–7% solubility (Sholkovitz et al., 2010). Values are lower than those measured on three GEOTRACES cruises in the North Atlantic, where Cu solubility ranged from ~1–50%, with a median of ~15% (Shelley et al. 2018). It is possible that these higher values reflect the input of anthropogenic aerosols (Sholkovitz et al., 2010).

While Fe limitation characterizes 30–40% of the world ocean (Sunda 2012), other bioactive metals play important roles in fostering phytoplankton growth and influencing species compositions, and may be co-limiting in certain regions (Moore et al. 2013). For example, the addition of Mn, Cu, and Zn in bottle experiments in the subarctic Pacific stimulated algal growth (Coale 1991; Crawford et al. 2003). Zinc may be co-limiting in this region because of particularly low concentrations in surface waters (Lohan et al. 2002). Co was found to be co-limiting with Fe in the GOA during the VERTEX experiment (Martin et al. 1989). Copper also can be co-limiting with Fe, as Cu is needed for Fe uptake (Peers et al., 2005). Metal availability also plays a role in driving species compositions, as metal requirements differ among taxa (e.g., Twining and Baines, 2013). For instance, high Zn concentrations can support the growth of coccolithophores, which have a high Zn requirement (Sunda and Huntsman 1995). Given that Co and Cd can substitute into Zn-containing enzymes such as carbonic anhydrase and alkaline phosphatase, their presence may support growth when Zn concentrations are low (Price and Morel 1990; Lee and Morel 1995; Sunda and Huntsman 1995). We found that glacier-derived dust supplies relatively high concentrations of metals such as Cu, Zn, and Co compared to volcanic ash, suggesting that Alaska dust may be an important source of these nutrients to offshore waters.

4.3 Potential toxicity

In terms of potential toxicity, Pb concentrations were five times higher in glacier-derived sediments (~30 ppm) than in volcanic ash (~6 ppm). Cu concentrations followed the same pattern: ~200 ppm in silt/loess samples and ~40 ppm in ash samples. We can use these concentrations, along with our median measured Cu solubility of 4.3%, to estimate total and/or soluble metal delivery during dust/ash deposition events of different sizes. For instance, Crusius et al. (2011) estimated that a single dust storm emanating from the Copper River valley into the Gulf of Alaska in November 2006 delivered 30–80 kton of dust. Using our values, this equates to 0.8–2.4 tons of total Pb, 5–16 tons of total Cu, and 0.2–0.7 tons of soluble Cu. Cu toxicity in phytoplankton has been reported at concentrations of 11 to 200 ppm in the water (Mann et al., 2002), while Pb toxicity has been found at 20–465 ppb and Cd toxicity at 0.23 to 500 ppb (Echeveste et al., 2012). Given the area over which dust from a single storm gets deposited, it seems unlikely an event such as this would reach the threshold necessary to cause toxic effects. This interpretation is consistent with an analysis of Saharan dust deposition in the tropical and subtropical Atlantic, where solubilities are similar (1–7%) but fluxes are much higher (Sholkovitz et al., 2010).

In contrast, a volcanic eruption can deliver an enormous volume of ash to the surface ocean in a short period of time, particularly in coastal waters (e.g., Olgun et al., 2011; Hoffmann et al., 2012). While events such as the 2008 eruption of Kasatochi (Alaska) and 2010 eruption of Eyjafjallajökull (Iceland) have been credited with triggering phytoplankton blooms through Fe fertilization (Hamme et al., 2010; Langmann et al., 2010; Achterberg et al., 2013), they also may supply large amounts of toxic metals to the atmosphere and ocean (e.g., Hoffmann et al., 2012; Edmonds et al., 2018). For instance, during the VEI 4 Kasatochi eruption, an estimated 0.15 to 0.28 km^3 of ash was erupted (Waythomas et al., 2010). Using our measured Pb and Cu concentrations from Pavlof and Redoubt ash samples, and an estimated density for volcanic ash of 1600 kg/m^3, we estimate that this event could have produced ~1400–2600 metric tons of total Pb, ~9,000–18,000 metric tons of total Cu, and 400–800 metric tons of soluble Cu. These estimates are comparable to, or somewhat higher than, estimates of total metal fluxes from the 2008 VEI 4 Chaitén eruption (Chile), which was rhyolitic (Ruggieri et al., 2012). Depending on the timeframe and area over which ash is deposited, these masses of toxic metals have the potential to cause negative effects on ecosystems (Hoffmann et al., 2012; Ruggieri et al., 2012).

4.4 Impacts of aging on sediment and ash Fe geochemistry

Aged samples tended to have higher proportions of exchangeable, easily-reducible, and reducible Fe compared to fresh samples (Figs. 6, 7). In the case of sediments, we were able to compare Holocene-aged loess (i.e., sampled from outcrops ^{14}C-dated by Muhs et al., 2013) to modern glaciofluvial samples. The loess samples had detectable Fe in the exchangeable fraction, as high as 1.7% of total Fe (median: 0.50 ± 0.41% MAD), whereas the glaciofluvial silts had essentially no Fe in this fraction (median: 0.06 ± 0.05% MAD). The loess samples had a 1.8 times higher proportion of easily-reducible Fe, at 33 ± 16% MAD compared to 19 ± 6.6% MAD for silt. Loess also had eight times higher Fe in the reducible fraction compared to silt, though with substantial variability (median: 9.8 ± 8.1% MAD compared to 1.2 ± 0.44%). The differences between fresh and aged ash were greater. Aged ash (spanning 8730 B.P. to 1990 C.E.) contained nearly twenty times higher easily-reducible Fe (median: 33.5 ± 2.2% MAD compared to 1.7 ± 0.2%) and over thirty times higher reducible Fe (median: 9.8 ± 8.2% MAD vs. 0.18 ± 0.08%) compared to fresh ash. These differences are consistent with the Fe solubility data, which show that aged ash samples contain six times more soluble Fe than fresh ash samples (Fig. 4; median: 0.28 ± 0.12% MAD vs. 0.04 ± 0.02% MAD). Thus, overall, the aged samples contained higher proportions of Fe fractions considered relevant to ecosystems.

The observed increases in exchangeable, easily-reducible, and reducible Fe in aged samples may relate to pedogenic processes as sediment or ash sits at the surface for decades to millennia. Soil development processes in the boreal forests of southcentral Alaska (including all our sample sites) are characterized by high annual precipitation (~400–1000 mm yr^{-1}), low pH (4–5), and the presence of chelates that allow Al and Fe migration (Carter and Pendleton, 1956; Stafford et al., 2000; Muhs et al., 2004). The detection of reducible Fe oxides by citrate-buffered sodium dithionite extraction (as in this study) has been used to infer the accumulation of Fe in soil B horizons (Muhs et al., 2004 and refs therein). In fact, the increase of reducible Fe can be used to predict age of sediment on the land surface (Dethier et al., 2012). Thus, the observed increases in the proportions of easily-reducible and reducible Fe fractions likely represent migration and accumulation of Fe in the sediment profile through time. Because of high loess accumulation rates at the sites we sampled (Muhs et al., 2003, 2013), deposition typically outpaces pedogenesis (Muhs et al., 2004). Nevertheless, our data provide evidence for changes in Fe geochemistry through time in the climate of southcentral Alaska. These changes are likely to

make the Fe within sediment/ash more accessible to organisms, either in situ or in the ocean, if this material were to become re-mobilized.

In the case of the ash samples, we only measured one set of paired fresh and aged samples, from Redoubt (1990 and 2009). The other aged samples (dated to 8730 B.P. to 3460 B.P.; Table 2) were erupted from Augustine, and we do not have an equivalent fresh sample. Therefore, we cannot discount geochemical variations among the volcanoes as a source of some of the observed differences between fresh and aged samples. However, the consistency of the pattern between both sediment and ash samples suggests that geochemical transformations are increasing Fe bioavailability through time. Future work can test this hypothesis by measuring additional paired aged and fresh ash samples from the same volcano(es).

4.5 Ash remobilization as a source of Fe to the ocean

Given the observed changes in ash Fe solubility and speciation as a result of environmental aging processes, the remobilization of aged volcanic ash may act as a mechanism of Fe delivery to HNLC waters. While volcanic eruptions are episodic and lack seasonality, remobilization events are subject to weather and climate patterns, and thus appear to exhibit seasonality. For instance, of 115 ash plumes observed from eight Kamchatka volcanoes over a 16-year period (2000–2016), 19 were determined to be remobilized ash, based on particle characteristics (Flower and Kahn 2017a,b). Importantly, the remobilization events occurred most frequently from July to early November, a time when adequate light is available to support phytoplankton blooms, provided that macronutrients are also in sufficient supply. The timing of these events likely depends on the desiccation of ash on the volcanoes' flanks during the summer months (Flower, pers. comm., 2017), which is likely a function of both temperature and the amount and type of precipitation. Further work is needed to assess the influences of temperature, precipitation, and winds on remobilization event frequency, timing, and magnitude.

4.6 Glaciogenic Fe delivery to the northeastern subarctic Pacific

Through a comparison of mineralogy, Fe and trace metal content and solubility, and Fe speciation, we have shown that glacier-derived materials have greater fertilization potential per unit mass than either Asian desert-derived dust or Aleutian Arc volcanic ash. These results support previous work which showed that dust derived through mechanical weathering processes

739 is more soluble, and provides particulate ferrous Fe which can be used by phytoplankton
740 (Schroth et al., 2009, 2011; Shoenfelt et al., 2017, 2019). While geologic source and weathering
741 history appear to dictate the geochemical properties of dust near its source region, additional
742 processing during atmospheric transport can significantly affect particulate geochemistry. In
743 particular, aerosol pH, condensation/evaporation cycles, the presence of ligands, and
744 photochemical reactions can impact Fe oxidation state and solubility, and subsequent
745 bioavailability (e.g., Duce and Tindale 1991; Cwiertny et al. 2008; Shi et al. 2009; Solmon et al.
746 2009; Chen and Grassian 2013). Natural aerosols also can mix with combustion products,
747 increasing overall Fe solubility (Sedwick et al. 2007; Sholkovitz et al. 2012). For these reasons,
748 particulate properties at their sources may not fully reflect downstream geochemistry. Future
749 work could assess the impact of atmospheric processing on dust from different source regions
750 (e.g., Asian deserts vs. Alaska glacier-fed riverbeds) to understand whether differences in
751 mineralogy and Fe speciation, as described in this study, persist through time.
752 A second largely unconstrained issue is that of flux. Marine sediment core-tops show that
753 recent dust fluxes across most of the subarctic North Pacific are in the range 1–2 $g/m^2/yr$ (Serno
754 et al. 2014). Eolian dust accounts for 80–100% of lithogenic flux at open-ocean sites far from
755 volcanic sources, and less than 50% near continental margins, where higher fluxes, differing
756 geochemistry, and coarser grain size modes point to terrigenous input, including volcanism
757 (Serno et al. 2014). Further investigation into dust provenance and deposition rates in the Gulf of
758 Alaska are needed in order to assess the flux from Alaska glaciofluvial sources, and the relative
759 magnitudes of deposition from local vs. Asian dust sources. Loess mass accumulation rates
760 (MARs) (<20 μm grain size) over the past 9,000 years at the Chitina loess section (Fig. 1) are in
761 the range 78–158 $g/m^2/yr$ (Muhs et al., 2013), significantly higher than the open-ocean fluxes
762 reported by Serno et al. (2014). This high rate of aeolian deposition within the Copper River
763 basin suggests that this region has been an active dust source throughout the Holocene.
764 Glaciogenic Fe fertilization in the offshore GOA may have been higher during times of
765 expanded glacier extents over the Pleistocene. Müller et al. (2018) found that peaks in primary
766 production from 1.5 to 0.5 Ma at IODP Site U1417 (northcentral GOA) corresponded with times
767 of increased glacially-sourced Fe input, both through ice-rafted detritus (IRD) and dust. Dust-
768 related productivity peaked several times across the Mid-Pleistocene Transition (MPT) (Müller
769 et al., 2018), likely related to increased glacial erosion (Gulick et al., 2015). As the Cordilleran

Ice Sheet expanded, dust-driven productivity peaks tapered off, while IRD-driven peaks persisted, likely reflecting an increase in marine-terminating glaciers (Müller et al., 2018). Farther to the south, McDonald et al. (1999) observed episodic extreme production events during MIS 5.3 to MIS 3 at ODP Site 887 (southcentral GOA), characterized by high Ba/Al and Si/Al, and diatom oozes up to ~1 m thick. The diatom-rich layers did not contain IRD, and the authors inferred that meltwater pulses or dust-borne Fe promoted the large blooms (McDonald et al., 1999). While neither study found a clear glacial-interglacial pattern in Fe fertilization events related to glaciation, it seems plausible that dust-driven events would be most likely to occur following intervals of glacial retreat, when ample glacial flour is available for deflation (Bullard, 2013). High loess MARs would appear to support this hypothesis, although it is important to bear in mind that MARs reflect both sediment production and loess accumulation processes (e.g., vegetation trapping dust) (Muhs et al., 2003; 2013)), and thus are not a perfect proxy for long-range dust transport.

Looking to the future, there are likely to be changes in glaciogenic sediment supply and mobilization in the GOA as a result of climate change, considering that nearly 30% of watershed area is covered by permanent snow and ice (Wang et al., 2004). For example, Schroth et al. (2011) demonstrated that the size, speciation, and mineralogy of Fe-bearing sediments differed between glaciated catchments and boreal-forested catchments within the Copper River basin, with the former dominated by Fe-bearing silicates, and the latter by Fe (hydr)oxides and Fe complexes with humic substances. Overall, their work suggested that fundamental changes in Fe geochemistry and supply in rivers will occur as deglaciation and reforestation continue. Likewise, the riverine supply of major nutrients including carbon, nitrogen, and phosphorus is likely to change as a result of deglaciation and reforestation (Hood and Scott, 2008). A year-long study of nutrient loads and river discharge in southeastern Alaska found that nonglaciated catchments yielded lower soluble reactive phosphorus fluxes and less labile dissolved organic matter than glaciated catchments (Hood and Scott, 2008). These changes in river-borne nutrients, particularly colloidal and particulate phases, are likely to affect the geochemistry and supply of aeolian dust deflated from riverbeds.

Changes in the timing of precipitation also may influence dust emissions. Peak stream flows in snowmelt-dominated rivers of central Alaska have shifted earlier by ~15–20 days over the past half-century (Stewart et al. 2005). It seems likely that ongoing reductions in seasonal

801 snow cover (e.g., Wipf et al. 2009) and increases in rain vs. snow (e.g., Karl et al. 1993) will
802 drive dust emissions ever earlier. Even a shift of 1–2 months would allow nutrient deposition to
803 coincide more closely with light availability, increasing the potential impact of local dust-derived
804 nutrients on phytoplankton in this HNLC region (e.g, Brickley and Thomas, 2004).
805 Dust delivery to offshore GOA waters is a function not only of fine-grained sediment
806 supply, but also of transport. Dust emission from the Copper River occurs primarily in the
807 autumn, when river discharge is low and before snow blankets the landscape (Crusius et al.,
808 2011), although transport has also been observed during springtime (Schroth et al., 2017).
809 Offshore dust transport requires northerly to northeasterly winds, which are driven by patterns of
810 anomalous high pressure in the Bering Sea and low pressure in the North Pacific (Crusius et al.,
811 2011; Schroth et al., 2017). Specifically, a more southerly position of the wintertime Aleutian
812 Low pressure system (ALow) facilitates dust transport into the GOA (Schroth et al., 2017). The
813 ALow has intensified over recent centuries, likely in response to warming tropical sea surface
814 temperatures (Osterberg et al., 2017). This intensification likely contributes to the observed
815 strong interannual variability in offshore dust transport (Schroth et al., 2017).
816
817 **5 Conclusions**
818 We conducted a variety of geochemical procedures to determine relative Fe fertilization
819 potential among four types of samples: glacier-derived silt and loess and fresh and aged ash
820 samples. We compared the findings to published data on Asian desert sediments. The results
821 from mineralogical, Fe extraction, and Fe solubility experiments were broadly consistent,
822 pointing to Alaska glacier-derived sediments as having the highest Fe fertilization potential
823 among these sample types. Specifically, we found the following:
824
825 1. Glacier-derived sediments have the highest weight percentages of easily-reducible iron,
826 five times higher than Asian desert sediments and fourteen times higher than fresh
827 volcanic ash. They also have twice as high Fe extracted from sheet silicates, mainly
828 chlorite.
829

2. Volcanic ash samples have the lowest available Fe and least soluble Fe of our samples, suggesting that volcanic ash fertilization may be a function of amount, rather than of favorable Fe geochemistry.

3. Alaska glacier-derived sediments contain five to thirty times higher Cu, Ni, and Pb than volcanic ash, and ~twice as high Co, Zn, Cd, and Mo, suggesting that dust-supplied bioactive metals may help support phytoplankton growth and influence species compositions in offshore waters.

4. Estimated delivery of Pb, Cu, and Cd during local dust storms is unlikely to cross a toxicity threshold, but the greater masses delivered during explosive volcanic eruptions may reach levels toxic to phytoplankton, depending on the rate and area of deposition.

5. Sediment Fe availability increases through environmental exposure in this climate, as evidenced by increased exchangeable and easily-reducible Fe fractions in the Holocene loess and ash samples compared to recent silt and fresh ash.

While this study has shown that local glacially-sourced material may have more Fe fertilization potential in the northeastern subarctic Pacific than long-traveled Asian dust or local volcanic eruptions, a critical factor that remains largely unconstrained is the fluxes of these aerosols to offshore regions. Future work should attempt to determine relative magnitudes of deposition to quantify the roles of these different nutrient sources in supporting this HNLC ecosystem.

Acknowledgments

We thank Colby undergraduates Jared Fong, Lily Sethares, Emily Visco, and Lilly Naimie, and Dartmouth undergraduates Rachel Rubin and Shoshanna Geller for their assistance in the lab. Thanks to Karina Graeter and Erin McConnell for help with field sampling. Thank you to Allan Brendell of Nelson Lagoon, AK and Michael Mungoven of Homer, AK for collecting and shipping ash samples to AVO (AT-3680 and AT-3982 respectively). We appreciate Mike Handley's assistance with ICP-MS analysis. Thanks also go to Whitney King, Karen Stamieszkin, Ben Twining, and Walter "Bill" Sullivan for helpful conversations and guidance. We gratefully acknowledge Colby College, the Buck Lab for Climate and Environment, and the

Dartmouth College Society of Fellows Postdoctoral Fellowship for supporting this research. Data have been uploaded to the EarthChem database and will be made available publicly upon paper acceptance. We thank the reviewers for their thoughtful feedback.

Figure Captions

Figure 1. Map showing sample sites in Alaska and the Yukon Territory, including the Chitina loess section and Copper River basin. Map generated using GeoMapApp.

Figure 2. Flowchart diagram showing sample processing and analysis steps used in this study. Not all samples went through all procedures.

Figure 3. Particle volume size distributions (dV/dlnD). Size-separated sediments have volume mode diameters of ~4–4.5 μm, while pristine ash samples, which were not size-separated, have volume mode diameters of ~10–11 μm. Aged ash samples are a bit coarser, with mode diameters of ~20 μm.

Figure 4. Cumulative fractional Fe solubility following successive leaches of sediment/ash samples with Milli-Q water. Fresh volcanic ash samples are ~7x less soluble than aged ash, loess, and glaciofluvial silt samples (calculated using median values), which all have similar Fe solubility. Samples were leached in triplicate, and error bars represent one standard deviation.

Figure 5. Box-and-whisker plots showing concentrations of bioactive and/or potentially toxic trace metals among four sample types. Boxes represent 25^{th} and 75^{th} percentiles, while the thin horizontal line shows the median value of each dataset. Whiskers (thin vertical lines) indicate the data range, excluding statistical outliers (outside ~2.7σ). Trace metals generally follow one of two patterns: Ni (A), Cu (B), and Pb (C) are 5–30x higher in loess and silt samples than in ash samples. Concentrations of Zn (D), Co (E), Cd (F), and Mo (G) are much more similar among samples, though glacier-derived samples remain higher than ashes. Mn (H) is slightly higher in fresh volcanic ash samples than in silt samples, while loess and aged ash have lower but similar concentrations.

Figure 6. Stacked bar plot showing proportions of total Fe represented by each Fe extractant. Color hues represent sample type, with tints indicating the Fe extraction used (see legend). Asian desert sediment bars represent means of samples from each desert (numbers given in parentheses) (Lu et al., 2017). Glaciofluvial silt, loess and aged ash samples have the highest proportions of easily-reducible Fe, while Asian sediments have the highest proportion of Fe as reducible Fe oxides. The majority of Fe in fresh volcanic ash samples is refractory.

Figure 7. Estimation plots of sequential Fe extraction data after Ho et al. (2019). Upper panels show distributions of values as % of total Fe represented by each extractant, with error bars giving the mean (black dot) and one standard deviation of each dataset. Lower panels show the average difference between each sample type and Asian desert sediment (from Lu et al., 2017). Error bars give 95% confidence intervals of the delta values. A) Fresh ash samples have lower easily-reducible Fe than Asian desert sediments, while aged ash, silt, and loess samples have ~3x higher easily-reducible Fe than desert sediments. B) Asian desert sediments have the highest proportion of reducible Fe oxides, ~3x higher than Alaska ash and sediment samples. C) Glaciofluvial silt samples have 2x higher proportions of Fe contained as sheet silicates and (oxy)hydroxides than Asian desert sediments and fresh and aged ashes. D) Fresh volcanic ash has ~3x higher refractory Fe than other sample types. Exchangeable Fe ($MgCl_2$ extraction) data are not shown, as this fraction was only detected in three loess samples.

Figure 8. Comparison of total extracted Fe to total digested Fe for independently processed and analyzed samples measured in this study and Asian desert sediments analyzed by Lu et al. (2017). Most samples fall near the 1:1 line, though several are significantly different between the two approaches.

Figure 9. Representative XRD spectra showing mineralogy of A) glacier-derived silt and loess samples and B) fresh volcanic ash samples. Chlorite appears as the dominant Fe-bearing mineral in glacier-derived samples, while ash samples do not contain any obvious Fe-bearing minerals.

Tables

Table 1. Sample locations, types, descriptions and major and trace element concentrations. IGSN stands for International Geo Sample Number and is a unique sample identifier. Nr indicates not reported. Major elements are reported as oxide weight percentages. Trace element concentrations are reported in ppm.

Table 2. AMS radiocarbon ages and calibrated age ranges for buried soils constraining the age of tephra layers on Augustine volcano.

Table 3. Cumulative fractional solubility data following successive leaches with a total volume of 1000 mL of Milli-Q water. Nr indicates not reported.

Table 4. Fe extraction data reported as weight % and as proportion of total Fe. Asian desert data represent average values from each desert (Lu et al 2017).

References

Achterberg, E. P., Moore, C. M., Henson, S. A., Steigenberger, S., Stohl, A., Eckhardt, S., . . . Klar, J. K. (2013). Natural iron fertilization by the Eyjafjallajökull volcanic eruption. *Geophysical Research Letters, 40*(5), 921-926.

Aguilar-Islas, A. M., Rember, R. D., Mordy, C. W., & Wu, J. (2008). Sea ice-derived dissolved iron and its potential influence on the spring algal bloom in the Bering Sea. *Geophysical Research Letters, 35*(24). doi:10.1029/2008GL035736

Ayris, P., & Delmelle, P. (2012). Volcanic and atmospheric controls on ash iron solubility: A review. *Physics and Chemistry of the Earth, Parts A/B/C, 45*, 103-112.

Baeyens, W., Bowie, A. R., Buesseler, K., Elskens, M., Gao, Y., Lamborg, C., . . . Zhang, H. (2011). Size-fractionated labile trace elements in the Northwest Pacific and Southern Oceans. *Marine Chemistry, 126*(1-4), 108-113.

Baker, A. R., Li, M., & Chance, R. (2020). Trace metal fractional solubility in size-segregated aerosols from the tropical eastern Atlantic Ocean. *Global Biogeochemical Cycles, 34*(6), e2019GB006510.

Bishop, J. K. B., Davis, R. E., & Sherman, J. T. (2002). Robotic observations of dust storm enhancement of carbon biomass in the North Pacific. *Science, 298*, 817-821.

Brickley, P. J., & Thomas, A. C. (2004). Satellite-measured seasonal and inter-annual chlorophyll variability in the Northeast Pacific and coastal Gulf of Alaska. *Deep-Sea Research II, 51*(1-2), 229-245. doi:10.1016/j.dsr2.2003.06.003

Browning, T. J., Bouman, H. A., Henderson, G. M., Mather, T. A., Pyle, D. M., Schlosser, C., . . . Moore, C. M. (2014). Strong responses of Southern Ocean phytoplankton communities to volcanic ash. *Geophysical Research Letters, 41*. doi:10/1002/2014GL059364

961 Browning, T. J., Stone, K., Bouman, H. A., Mather, T. A., Pyle, D. M., Moore, C. M., &
962 Martinez-Vicente, V. (2015). Volcanic ash supply to the surface ocean - remote sensing
963 of biological responses and their wider biogeochemical significance. *Frontiers in Marine*
964 *Science, 2*(14). doi:10.3389/fmars.2015.00014
965 Buck, C. S., Landing, W. M., & Resing, J. (2013). Pacific Ocean aerosols: Deposition and
966 solubility of iron, aluminum, and other trace elements. *Marine Chemistry, 157*, 117-130.
967 Bullard, J. E. (2013). Contemporary glacigenic inputs to the dust cycle. *Earth Surface Processes*
968 *and Landforms, 38*(1), 71-89.
969 Bullard, J. E., Baddock, M., Bradwell, T., Crusius, J., Darlington, E., Gaiero, D., . . . McCulloch,
970 R. (2016). High-latitude dust in the Earth system. *Reviews of Geophysics, 54*(2), 447-485.
971 Carter, G. F., & Pendleton, R. L. (1956). The humid soil: process and time. *Geographical*
972 *Review, 46*(4), 488-507.
973 Chen, H., & Grassian, V. H. (2013). Iron dissolution of dust source materials during simulated
974 acidic processing: The effect of sulfuric, acetic, and oxalic acids. *Environmental Science*
975 *& Technology, 47*(18), 10312-10321.
976 Chester, R., & Hughes, M. (1967). A chemical technique for the separation of ferro-manganese
977 minerals, carbonate minerals and adsorbed trace elements from pelagic sediments.
978 *Chemical Geology, 2*, 249-262.
979 Chuang, P. Y., Duvall, R. M., Shafer, M. M., & Schauer, J. J. (2005). The origin of water soluble
980 particulate iron in the Asian atmospheric outflow. *Geophysical Research Letters,*
981 *32*(L07813). doi:10.1029/2004GL021946
982 Coale, K. H. (1991). Effects of iron, manganese, copper, and zinc enrichments on productivity
983 and biomass in the subarctic Pacific. *Limnology and Oceanography, 36*(8), 1851-1864.
984 Crawford, D., Lipsen, M., Purdie, D., Lohan, M., Statham, P., Whitney, F., . . . Peterson, T.
985 (2003). Influence of zinc and iron enrichments on phytoplankton growth in the
986 northeastern subarctic Pacific. *Limnology and Oceanography, 48*(4), 1583-1600.
987 Crusius, J., Schroth, A. W., Gasso, S., Moy, C. M., Levy, R. C., & Gatica, M. (2011). Glacial
988 flour dust storms in the Gulf of Alaska: Hydrologic and meteorological controls and their
989 importance as a source of bioavailable iron. *Geophysical Research Letters, 38*(L06602).
990 doi:10.1029/2010GL046573
991 Cwiertny, D. M., Young, M. A., & Grassian, V. H. (2008). Chemistry and photochemistry of
992 mineral dust aerosol. *Annu. Rev. Phys. Chem., 59*, 27-51.
993 Dethier, D. P., Birkeland, P. W., & McCarthy, J. A. (2012). Using the accumulation of CBD-
994 extractable iron and clay content to estimate soil age on stable surfaces and nearby
995 slopes, Front Range, Colorado. *Geomorphology, 173*, 17-29.
996 Duce, R. A., & Tindale, N. W. (1991). Atmospheric Transport of Iron and its Deposition in the
997 Ocean. *Limnology and Oceanography, 36*(8), 1715-1726.
998 Duggen, S., Olgun, N., Croot, P., Hoffmann, L., Dietze, H., Delmelle, P., & Teschner, C. (2010).
999 The role of airborne volcanic ash for the surface ocean biogeochemical iron-cycle: a
1000 review. *Biogeosciences, 7*, 827-844.
1001 Echeveste, P., Agustí, S., & Tovar-Sánchez, A. (2012). Toxic thresholds of cadmium and lead to
1002 oceanic phytoplankton: cell size and ocean basin–dependent effects. *Environmental*
1003 *Toxicology and Chemistry, 31*(8), 1887-1894.
1004 Edmonds, M., Mather, T. A., & Liu, E. J. (2018). A distinct metal fingerprint in arc volcanic
1005 emissions. *Nature Geoscience, 11*(10), 790-794.

1006 Fan, S., Moxim, W. J., & Levy II, H. (2006). Aeolian input of bioavailable iron to the ocean.
1007 *Geophysical Research Letters, 33*(L07602). doi:10.1029/2005GL024852
1008 Fischer, E. V., Hsu, N. C., Jaffe, D. A., Jeong, M.-J., & Gong, S. L. (2009). A decade of dust:
1009 Asian dust and springtime aerosol load in the U.S. Pacific Northwest. *Geophysical*
1010 *Research Letters, 36*(3). doi:10.1029/2008GL036467
1011 Flower, V. J. B., & Kahn, R. A. (2017a). Assessing the altitude and dispersion of volcanic
1012 plumes using MISR multi-angle imaging from space: Sixteen years of volcanic activity in
1013 the Kamchatka Peninsula, Russia. *Journal of Volcanology and Geothermal Research,*
1014 *337*, 1-15. doi:10.1016/j.jvolgeores.2017.03.010
1015 Flower, V. J. B., & Kahn, R. A. (2017b). Distinguishing remobilized ash from erupted volcanic
1016 plumes using space-borne multiangle imaging. *Geophysical Research Letters, 44*,
1017 10,772-710,779. doi:10.1002/2017GL074740
1018 Frogner, P., Gislason, S. R., & Oskarsson, N. (2001). Fertilizing potential of volcanic ash in
1019 ocean surface water. *Geology, 29*(6), 487-490.
1020 Global Volcanism Program. (2013). Volcanoes of the World, v. 4.9.0 (04 Jun 2020) (Publication
1021 no. 10.5479/si.GVP.VOTW4-2013). Retrieved 30 July 2019, from Smithsonian
1022 Institution
1023 Grebmeier, J. M., Overland, J. E., Moore, S. E., Farley, E. V., Carmack, E. C., Cooper, L. W., . .
1024 . McNutt, S. L. (2006). A major ecosystem shift in the northern Bering Sea. *Science, 311*,
1025 1461-1464.
1026 Greene, A. R., DeBARI, S. M., Kelemen, P. B., Blusztajn, J., & Clift, P. D. (2006). A detailed
1027 geochemical study of island arc crust: the Talkeetna arc section, south–central Alaska.
1028 *Journal of Petrology, 47*(6), 1051-1093.
1029 Gregg, W. W., Conkright, M. E., Ginoux, P., O'Reilly, J. E., & Casey, N. W. (2003). Ocean
1030 primary production and climate: Global decadal changes. *Geophysical Research Letters,*
1031 *30*(15,1809). doi:10.1029/2003GL016889
1032 Gulick, S. P., Jaeger, J. M., Mix, A. C., Asahi, H., Bahlburg, H., Belanger, C. L., . . . Drab, L.
1033 (2015). Mid-Pleistocene climate transition drives net mass loss from rapidly uplifting St.
1034 Elias Mountains, Alaska. *Proceedings of the National Academy of Sciences, 112*(49),
1035 15042-15047.
1036 Hamme, R. C., Webley, P. W., Crawford, W. R., Whitney, F. A., DeGrandpre, M. D., Emerson,
1037 S. R., . . . Lockwood, D. (2010). Volcanic ash fuels anomalous plankton bloom in
1038 subarctic northeast Pacific. *Geophysical Research Letters, 37*(L19604).
1039 doi:10.1029/2010GL044629
1040 Harrison, P. J., Boyd, P. W., Varela, D. E., Takeda, S., Shiomoto, A., & Odate, T. (1999).
1041 Comparison of factors controlling phytoplankton productivity in the NE and NW
1042 subarctic Pacific gyres. *Progress in Oceanography, 43*, 205-234.
1043 Heron, G., Crouzet, C., Bourg, A. C., & Christensen, T. H. (1994). Speciation of Fe (II) and Fe
1044 (III) in contaminated aquifer sediments using chemical extraction techniques.
1045 *Environmental Science & Technology, 28*(9), 1698-1705.
1046 Hildreth, W. (1983). The compositionally zoned eruption of 1912 in the Valley of Ten Thousand
1047 Smokes, Katmai National Park, Alaska. *Journal of Volcanology and Geothermal*
1048 *Research, 18*(1-4), 1-56.
1049 Ho, J., Tumkaya, T., Aryal, S., Choi, H., & Claridge-Chang, A. (2019). Moving beyond P
1050 values: data analysis with estimation graphics. *Nature methods, 16*(7), 565-566.

1051 Hoffmann, L. J., Breitbarth, E., Ardelan, M., Duggen, S., Olgun, N., Hassellöv, M., &
1052 Wängberg, S.-Å. (2012). Influence of trace metal release from volcanic ash on growth of
1053 Thalassiosira pseudonana and Emiliania huxleyi. *Marine Chemistry, 132*, 28-33.
1054 Hood, E., & Scott, D. (2008). Riverine organic matter and nutrients in southeast Alaska affected
1055 by glacial coverage. *Nature Geoscience, 1*(9), 583-587.
1056 Jickells, T., Baker, A., & Chance, R. (2016). Atmospheric transport of trace elements and
1057 nutrients to the oceans. *Philosophical Transactions of the Royal Society A: Mathematical,*
1058 *Physical and Engineering Sciences, 374*(2081), 20150286.
1059 Jickells, T., & Spokes, L. J. (2001). Atmospheric iron inputs to the oceans *The Biogeochemistry*
1060 *of Iron in Seawater* (pp. 85-121): J. Wiley.
1061 Jones, M. T., & Gislason, S. R. (2008). Rapid releases of metal salts and nutrients following the
1062 deposition of volcanic ash into aqueous environments. *Geochimica et Cosmochimica*
1063 *Acta, 72*, 3661-3680. doi:10.1016/j.gca.2008.05.030
1064 Journet, E., Desboeufs, K. V., Caquineau, S., & Colin, J. L. (2008). Mineralogy as a critical
1065 factor of dust iron solubility. *Geophysical Research Letters, 35*(7).
1066 Jweda, J., Bolge, L., Class, C., & Goldstein, S. L. (2015). High precision Sr-Nd-Hf-Pb isotopic
1067 compositions of USGS reference material BCR-2. *Geostandards and Geoanalytical*
1068 *Research*. doi:10.1111/j.1751-908X.2015.00342.x
1069 Karl, T. R., Groisman, P. Y., Knight, R. W., & Heim Jr., R. R. (1993). Recent variations of snow
1070 cover and snowfall in North America and their relation to precipitation and temperature
1071 variations. *Journal of Climate, 6*, 1327-1344.
1072 Kipp, L. E., Charette, M. A., Moore, W. S., Henderson, P. B., & Rigor, I. G. (2018). Increased
1073 fluxes of shelf-derived materials to the central Arctic Ocean. *Science, 4*(1,eaao1302).
1074 doi:10.1126/sciadv.aao1302
1075 Langmann, B., Zaksek, K., Hort, M., & Duggen, S. (2010). Volcanic ash as fertiliser for the
1076 surface ocean. *Atmospheric Chemistry and Physics, 10*, 3891-3899.
1077 Lee, J. G., & Morel, F. M. (1995). Replacement of zinc by cadmium in marine phytoplankton.
1078 *Marine Ecology Progress Series, 127*, 305-309.
1079 Lim, B., Jickells, T., Colin, J., & Losno, R. (1994). Solubilities of Al, Pb, Cu, and Zn in rain
1080 sampled in the marine environment over the North Atlantic Ocean and Mediterranean
1081 Sea. *Global Biogeochemical Cycles, 8*(3), 349-362.
1082 Lohan, M. C., Statham, P. J., & Crawford, D. W. (2002). Total dissolved zinc in the upper water
1083 column of the subarctic North East Pacific. *Deep Sea Research Part II: Topical Studies*
1084 *in Oceanography, 49*(24-25), 5793-5808.
1085 Lu, W., Zhao, W., Balsam, W., Lu, H., Liu, P., Lu, Z., & Ji, J. (2017). Iron mineralogy and
1086 speciation in clay-sized fractions of Chinese desert sediments. *Journal of Geophysical*
1087 *Research - Atmospheres, 122*. doi:10.1002/2017JD027733
1088 Mahowald, N., Baker, A. R., Bergametti, G., Brooks, N., Duce, R. A., Jickells, T. D., . . . Tegen,
1089 I. (2005). Atmospheric global dust cycle and iron inputs to the ocean. *Global*
1090 *Biogeochemical Cycles, 19*(4).
1091 Mahowald, N. M., Engelstaedter, S., Luo, C., Sealy, A., Artaxo, P., Benitez-Nelson, C., . . .
1092 Siefert, R. L. (2009). Atmospheric Iron Deposition: Global Distribution, Variability and
1093 Human Perturbations. *Annual Review of Marine Science, 14*(33).
1094 Mann, E. L., Ahlgren, N., Moffett, J. W., & Chisholm, S. W. (2002). Copper toxicity and
1095 cyanobacteria ecology in the Sargasso Sea. *Limnology and Oceanography, 47*(4), 976-
1096 988.

1097 Martin, J. H., Gordon, R. M., Fitzwater, S., & Broenkow, W. W. (1989). VERTEX:
1098 phytoplankton/iron studies in the Gulf of Alaska. *Deep Sea Research Part A.*
1099 *Oceanographic Research Papers, 36*(5), 649-680.
1100 McDonald, D., Pedersen, T., & Crusius, J. (1999). Multiple late Quaternary episodes of
1101 exceptional diatom production in the Gulf of Alaska. *Deep Sea Research Part II: Topical*
1102 *Studies in Oceanography, 46*(11-12), 2993-3017.
1103 Measures, C. I., Brown, M. T., & Vink, S. (2005). Dust deposition to the surface waters of the
1104 western and central North Pacific inferred from surface water dissolved aluminum
1105 concentrations. *Geochemistry, Geophysics, Geosystems, 6*(9).
1106 doi:10.1029/2005GC000922
1107 Mehra, O. P., & Jackson, M. L. (1958). Iron Oxide Removal from Soils and Clays by a
1108 Dithionite-Citrate System Buffered with Sodium Bicarbonate. *Clays and Clay Minerals,*
1109 *7*(1), 317-327. doi:10.1346/CCMN.1958.0070122
1110 Moore, C., Mills, M., Arrigo, K., Berman-Frank, I., Bopp, L., Boyd, P., . . . Jaccard, S. (2013).
1111 Processes and patterns of oceanic nutrient limitation. *Nature Geoscience, 6*(9), 701-710.
1112 Moore, D. M., & Reynolds Jr, R. C. (1989). *X-ray Diffraction and the Identification and*
1113 *Analysis of Clay Minerals*: Oxford University Press (OUP).
1114 Morel, F. M., Rueter, J. G., & Price, N. M. (1991). Iron nutrition of phytoplankton and its
1115 possible importance in the ecology of ocean regions with high nutrient and low biomass.
1116 *Oceanography, 4*(2), 56-61.
1117 Muhs, D. R., A., A. T., Bettis III, E. A., McGeehin, J., Been, J. M., Begét, J. E., . . . De Anne, S.
1118 P. (2003). Stratigraphy and palaeoclimatic significance of Late Quaternary loess–
1119 palaeosol sequences of the Last Interglacial–Glacial cycle in central Alaska. *Quaternary*
1120 *Science Reviews, 22*(18-19), 1947-1986.
1121 Muhs, D. R., Budahn, J. R., McGeehin, J. P., Bettis III, E. A., Skipp, G., Paces, J. B., & Wheeler,
1122 E. A. (2013). Loess origin, transport, and deposition over the past 10,000 years,
1123 Wrangell-St. Elias National Park, Alaska. *Aeolian Research, 11*, 85-99.
1124 Muhs, D. R., McGeehin, J. P., Beann, J., & Fisher, E. (2004). Holocene loess deposition and soil
1125 formation as competing processes, Matanuska Valley, southern Alaska. *Quaternary*
1126 *Research, 61*(3), 265-276.
1127 Müller, J., Romero, O., Cowan, E. A., McClymont, E. L., Forwick, M., Asahi, H., . . . Mix, A.
1128 (2018). Cordilleran ice-sheet growth fueled primary productivity in the Gulf of Alaska,
1129 northeast Pacific Ocean. *Geology, 46*(4), 307-310.
1130 Olgun, N., Duggen, S., Croot, P. L., Delmelle, P., Dietze, H., Schacht, U., . . . Garbe-Schönberg,
1131 D. (2011). Surface ocean iron fertilization: The role of airborne volcanic ash from
1132 subduction zone and hot spot volcanoes and related iron fluxes into the Pacific Ocean.
1133 *Global Biogeochemical Cycles, 25*(4).
1134 Olgun, N., Duggen, S., Langmann, B., Hort, M., Waythomas, C. F., Hoffmann, L., & Croot, P.
1135 (2013). Geochemical evidence of oceanic iron fertilization by the Kasatochi volcanic
1136 eruption in 2008 and the potential impacts on Pacific sockeye salmon. *Marine Ecology*
1137 *Progress Series, 488*, 81-88. doi:10.3354/meps10403
1138 Osterberg, E. C., Winski, D. A., Kreutz, K. J., Wake, C. P., Ferris, D. G., Campbell, S., . . .
1139 Birkel, S. D. (2017). The 1200 year composite ice core record of Aleutian Low
1140 intensification. *Geophysical Research Letters, 44*. doi:10.1002/2017GL073697

1141 Parsons, T. R., & Whitney, F. A. (2012). Did volcanic ash from Mt. Kasatoshi in 2008 contribute
1142 to a phenomenal increase in Fraser River sockeye salmon (Oncorhynchus nerka) in 2010?
1143 *Fisheries Oceanography, 21*(5), 374-377.
1144 Paytan, A., Mackey, K. R. M., Chen, Y., Lima, I. D., Doney, S. C., Mahowald, N., . . . Post, A.
1145 F. (2009). Toxicity of atmospheric aerosols on marine phytoplankton. *Proceedings of the*
1146 *National Academy of Sciences of the United States of America, 106*(12), 4601-4605.
1147 doi:10.1073/pnas.0811486106
1148 Peers, G., Quesnel, S. A., & Price, N. M. (2005). Copper requirements for iron acquisition and
1149 growth of coastal and oceanic diatoms. *Limnology and Oceanography, 50*(4), 1149-1158.
1150 Poulton, S. W., & Canfield, D. E. (2005). Development of a sequential extraction procedure for
1151 iron: implications for iron partitioning in continentally derived particulates. *Chemical*
1152 *Geology, 214*, 209-221.
1153 Poulton, S. W., & Raiswell, R. (2005). Chemical and physical characteristics of iron oxides in
1154 riverine and glacial meltwater sediments. *Chemical Geology, 218*(3-4), 203-221.
1155 Price, N., & Morel, F. (1990). Cadmium and cobalt substitution for zinc in a marine diatom.
1156 *Nature, 344*(6267), 658-660.
1157 Reimer, P. J., Baillie, M. G. L., Bard, E., Bayliss, A., Beck, J. W., Bertrand, C. J. H., . . .
1158 Weyhenmeyer, C. E. (2004). IntCal04 Terrestrial radiocarbon age calibration, 26 - 0 ka.
1159 *Radiocarbon, 46*(3), 1029-1058.
1160 Ruggieri, F., Fernandez-Turiel, J., Saavedra, J., Gimeno, D., Polanco, E., Amigo, A., . . . Caselli,
1161 A. (2012). Contribution of volcanic ashes to the regional geochemical balance: The 2008
1162 eruption of Chaitén volcano, Southern Chile. *Science of the Total Environment, 425*, 75-
1163 88.
1164 Schroth, A. W., Crusius, J., Chever, F., Bostick, B. C., & Rouxel, O. J. (2011). Glacial influence
1165 on the geochemistry of riverine iron fluxes to the Gulf of Alaska and effects of
1166 deglaciation. *Geophysical Research Letters, 38*(16).
1167 Schroth, A. W., Crusius, J., Gassó, S., Moy, C. M., Buck, N. J., Resing, J. A., & Campbell, R.
1168 W. (2017). Atmospheric deposition of glacial iron in the Gulf of Alaska impacted by the
1169 position of the Aleutian Low. *Geophysical Research Letters, 44*(10), 5053-5061.
1170 Schroth, A. W., Crusius, J., Sholkovitz, E. R., & Bostick, B. C. (2009). Iron solubility driven by
1171 speciation in dust sources to the ocean. *Nature Geoscience, 2*. doi:10.1038.NGEO501
1172 Sedwick, P. N., Sholkovitz, E. R., & Church, T. M. (2007). Impact of anthropogenic combustion
1173 emissions on the fractional solubility of aerosol iron: Evidence from the Sargasso Sea.
1174 *Geochemistry, Geophysics, Geosystems, 8*(10). doi:10.1029/2007GC001586
1175 Serno, S., Winckler, G., Anderson, R. F., Hayes, C. T., McGee, D., Machalett, B., . . . Haug, G.
1176 H. (2014). Eolian dust input to the Subarctic North Pacific. *Earth and Planetary Science*
1177 *Letters, 387*, 252-263.
1178 Serreze, M. C., Holland, M. M., & Stroeve, J. (2007). Perspectives on the Arctic's shrinking sea-
1179 ice cover. *Science, 315*, 1533-1536.
1180 Shelley, R. U., Landing, W. M., Ussher, S. J., Planquette, H., & Sarthou, G. (2018). Regional
1181 trends in the fractional solubility of Fe and other metals from North Atlantic aerosols
1182 (GEOTRACES cruises GA01 and GA03) following a two-stage leach. *Biogeosciences*,
1183 2271-2288.
1184 Shi, Z., Krom, M. D., Bonneville, S., Baker, A. R., Jickells, T. D., & Benning, L. G. (2009).
1185 Formation of iron nanoparticles and increase in iron reactivity in mineral dust during
1186 simulated cloud processing. *Environmental Science & Technology, 43*(17), 6592-6596.

1187 Shoenfelt, E. M., Sun, J., Winckler, G., Kaplan, M. R., Borunda, A. L., Farrell, K. R., . . .
1188 Bostick, B. C. (2017). High particulate iron(II) content in glacially sourced dusts
1189 enhances productivity of a model diatom. *Science Advances, 3*(6, e1700314).
1190 doi:10.1126/sciadv.1700314
1191 Shoenfelt, E. M., Winckler, G., Annett, A. L., Hendry, K. R., & Bostick, B. C. (2019). Physical
1192 weathering intensity controls bioavailable primary iron (II) silicate content in major
1193 global dust sources. *Geophysical Research Letters, 46*(19), 10854-10864.
1194 Sholkovitz, E. R., Sedwick, P. N., & Church, T. M. (2010). On the fractional solubility of copper
1195 in marine aerosols: Toxicity of aeolian copper revisited. *Geophysical Research Letters,*
1196 *37*(20).
1197 Sholkovitz, E. R., Sedwick, P. N., Church, T. M., Baker, A. R., & Powell, C. F. (2012).
1198 Fractional solubility of aerosol iron: Synthesis of a global-scale data set. *Geochimica et*
1199 *Cosmochimica Acta, 89*, 173-189. doi:10.1016/j.gca.2012.04.022
1200 Simonella, L. E., Palomeque, M., Croot, P., Stein, A., Kupczewski, M., Rosales, A., . . .
1201 Villarosa, G. (2015). Soluble iron inputs to the Southern Ocean through recent andesitic
1202 to rhyolitic volcanic ash eruptions from the Patagonian Andes. *Global Biogeochemical*
1203 *Cycles, 29*(8), 1125-1144.
1204 Slotznick, S., Sperling, E., Tosca, N., Miller, A., Clayton, K., Van Helmond, N., . . . Swanson-
1205 Hysell, N. (2020). Unraveling the mineralogical complexity of sediment iron speciation
1206 using sequential extractions. *Geochemistry, Geophysics, Geosystems, 21*(2),
1207 e2019GC008666.
1208 Solmon, F., Chuang, P. Y., Meskhidze, N., & Chen, Y. (2009). Acidic processing of mineral dust
1209 iron by anthropogenic compounds over the north Pacific Ocean. *Journal of Geophysical*
1210 *Research, 114*(D02305). doi:10.1029/2008JD010417
1211 Stafford, J., Wendler, G., & Curtis, J. (2000). Temperature and precipitation of Alaska: 50 year
1212 trend analysis. *Theoretical and Applied Climatology, 67*(1-2), 33-44.
1213 Stewart, I. T., Cayan, D. R., & Dettinger, M. D. (2005). Changes toward earlier streamflow
1214 timing across western North America. *Journal of Climate, 18*(8), 1136-1155.
1215 Stuiver, M., & Reimer, P. J. (1993). Extended 14 C data base and revised CALIB 3.0 14 C age
1216 calibration program. *Radiocarbon, 35*(1), 215-230.
1217 Sunda, W. (2012). Feedback interactions between trace metal nutrients and phytoplankton in the
1218 ocean. *Frontiers in Microbiology, 3*, 204.
1219 Sunda, W. G., & Huntsman, S. A. (1995). Iron uptake and growth limitation in oceanic and
1220 coastal phytoplankton. *Marine Chemistry, 50*, 189-206.
1221 Thuróczy, C.-E., Boye, M., & Losno, R. (2010). Dissolution of cobalt and zinc from natural and
1222 anthropogenic dusts in seawater. *Biogeosciences, 7*(6), 1927-1936.
1223 Twining, B. S., & Baines, S. B. (2013). The trace metal composition of marine phytoplankton.
1224 *Annual Review of Marine Science, 5*, 191-215.
1225 Twining, B. S., Baines, S. B., Bozard, J. B., Vogt, S., Walker, E. A., & Nelson, D. M. (2011).
1226 Metal quotas of plankton in the equatorial Pacific Ocean. *Deep Sea Research Part II:*
1227 *Topical Studies in Oceanography, 58*(3-4), 325-341.
1228 Uno, I., Eguchi, K., Yumimoto, K., Takemura, T., Shimizu, A., Uematsu, M., . . . Sugimoto, N.
1229 (2009). Asian dust transported one full circuit around the globe. *Nature Geoscience, 2*.
1230 doi:10.1038/NGEO583
1231 Wallace, K. L., & Schwaiger, H. F. (2018). Volcanic ash resuspension from the Katmai region.
1232 *Alaska Park Science, 18*(1), 62-69.

1233 Wang, J., Jin, M., Musgrave, D. L., & Ikeda, M. (2004). A hydrological digital elevation model
1234 for freshwater discharge into the Gulf of Alaska. *Journal of Geophysical Research:*
1235 *Oceans, 109*(C7).
1236 Waythomas, C. F., Scott, W. E., Prejean, S. G., Schneider, D. J., Izbekov, P., & Nye, C. J.
1237 (2010). The 7–8 August 2008 eruption of Kasatochi Volcano, central Aleutian Islands,
1238 Alaska. *Journal of Geophysical Research: Solid Earth, 115*(B12).
1239 Whitney, P. R. (1975). Relationship of manganese-iron oxides and associated heavy metals to
1240 grain size in stream sediments. *Journal of Geochemical Exploration, 4*(2), 251-263.
1241 Winton, V. H. L., Edwards, R., Delmonte, B., Ellis, A., Andersson, P. S., Bowie, A. R., . . .
1242 Tuohy, A. (2016). Multiple sources of soluble atmospheric iron to Antarctic waters.
1243 *Global Biogeochemical Cycles, 30*, 421-437. doi:10.1002/2016GB005265
1244 Wipf, S., Stoeckli, V., & Bebi, P. (2009). Winter climate change in alpine tundra: plant responses
1245 to changes in snow depth and snowmelt timing. *Climatic Change, 94*(1-2), 105-121.
1246 Wu, J., Boyle, E., Sunda, W., & Wen, L. (2001). Soluble and colloidal iron in the oligotrophic
1247 North Atlantic and North Pacific. *Science, 293*, 847-849.
1248 Xuan, J., & Sokolik, I. N. (2002). Characterization of sources and emission rates of mineral dust
1249 in Northern China. *Atmospheric Environment, 36*(31), 4863-4876. doi:10.1016/S1352-
1250 2310(02)00585-X
1251
1252